JPn Neuroscience

The Journal of Physiology

J Physiol 595.4 (2017) pp 1315–1337

Tonotopic action potential tuning of maturing auditory neurons through endogenous ATP

Saša Jovanovic[1], Tamara Radulovic[1,3], Claudio Coddou[2], Beatrice Dietz[1], Jana Nerlich[1,3], Stanko S. Stojilkovic[2], Rudolf Rübsamen[1] and Ivan Milenkovic[1,3]

[1] *Institute of Biology, Faculty of Biosciences, Pharmacy and Psychology, University of Leipzig, Leipzig, Germany*
[2] *Section on Cellular Signaling, Program in Developmental Neuroscience, National Institute of Child Health and Human Development, National Institutes of Health, Bethesda, MD, USA*
[3] *Carl Ludwig Institute for Physiology, Faculty of Medicine, University of Leipzig, Leipzig, Germany*

Key points

- Following the genetically controlled formation of neuronal circuits, early firing activity guides the development of sensory maps in the auditory, visual and somatosensory system. However, it is not clear whether the activity of central auditory neurons is specifically regulated depending on the position within the sensory map.
- In the ventral cochlear nucleus, the first central station along the auditory pathway, we describe a mechanism through which paracrine ATP signalling enhances firing in a cell-specific and tonotopically-determined manner.
- Developmental down-regulation of P2X2/3R currents along the tonotopic axis occurs simultaneously with an increase in AMPA receptor currents, suggesting a high-to-low frequency maturation pattern.
- Facilitated action potential (AP) generation, measured as higher firing rate, shorter EPSP-AP delay *in vivo* and shorter AP latency in slice experiments, is consistent with increased synaptic efficacy caused by ATP.
- The long lasting change in intrinsic neuronal excitability is mediated by the heteromeric P2X2/3 receptors.

Abstract Synaptic refinement and strengthening are activity-dependent processes that establish orderly arranged cochleotopic maps throughout the central auditory system. The maturation of auditory brainstem circuits is guided by action potentials (APs) arising from the inner hair cells in the developing cochlea. The AP firing of developing central auditory neurons can be modulated by paracrine ATP signalling, as shown for the cochlear nucleus bushy cells and principal neurons in the medial nucleus of the trapezoid body. However, it is not clear whether neuronal activity may be specifically regulated with respect to the nuclear tonotopic position (i.e. sound frequency selectivity). Using slice recordings before hearing onset and *in vivo* recordings with iontophoretic drug applications after hearing onset, we show that cell-specific purinergic modulation follows a precise tonotopic pattern in the ventral cochlear nucleus of developing gerbils. In high-frequency regions, ATP responsiveness diminished before hearing onset. In low-to-mid frequency regions, ATP modulation persisted after hearing onset in a subset of low-frequency bushy cells (characteristic frequency$<$ 10 kHz). Down-regulation of P2X2/3R currents along the tonotopic axis occurs simultaneously with an increase in AMPA receptor currents, thus suggesting a high-to-low frequency maturation pattern. Facilitated AP generation, measured as higher firing frequency, shorter EPSP-AP delay *in vivo*, and shorter AP latency in slice experiments, is consistent with increased synaptic efficacy caused by ATP. Finally, by combining recordings and pharmacology *in vivo*, in slices, and in human embryonic kidney 293 cells, it was shown that the long lasting change in intrinsic neuronal excitability is mediated by the P2X2/3R.

DOI: 10.1113/JP273272

(Received 10 August 2016; accepted after revision 2 November 2016; first published online 7 November 2016)
Corresponding author I. Milenkovic: Carl Ludwig Institute for Physiology, Faculty of Medicine, University of Leipzig, Liebigstrasse 27, 04103 Leipzig, Germany. Email: ivan.milenkovic@medizin.uni-leipzig.de

Abbreviations aCSF, artificial cerebrospinal fluid; AMPAR, AMPA receptor; AN, auditory nerve; AP, action potential; APhw, action potential half-width; AVCN, anteroventral cochlear nucleus; BCs, bushy cells; CF, characteristic frequency; CN, cochlear nucleus; GluR, glutamate receptor; HEK, human embryonic kidney 293; IHC, inner hair cell; ISI, interspike interval; MNTB, medial nucleus of the trapezoid body; PKC, protein kinase C; PN, principal neuron; PP, presynaptic action potential; PVCN, posteroventral cochlear nucleus; R_{in}, input resistance; RM, repeated measures; RT, room temperature; VCN, ventral cochlear nucleus; V_{hold}, holding potential.

Introduction

Information processing in the auditory, visual and somatosensory systems depends on the topographic organization of neuronal networks that form maps of receptor epithelia along the afferent pathways and in primary cortical areas (Friauf and Lohmann, 1999; Inan and Crair, 2007; White and Fitzpatrick, 2007; Cang and Feldheim, 2013). The development of sensory maps requires molecular guidance cues to create gross neuronal connections that are consecutively refined by the neuronal activity (O'Leary and McLaughlin, 2005; Butts *et al.* 2007; Hanganu-Opatz, 2010).

In the auditory system, neighboring inner hair cells (IHCs) are tuned to slightly different sound frequencies, giving rise to the cochlear tonotopic organization (Davis, 2003; Mann and Kelley, 2011). Before hearing onset, activity of adjacent IHCs is synchronized by paracrine ATP signalling from supporting cells of the Köllikers organ (Tritsch *et al.* 2007; Tritsch *et al.* 2010) and additionally modulated by the ACh release from efferent projections (Glowatzki and Fuchs, 2000; Johnson *et al.* 2011). The temporal structure of activity appears to provide relevant information for the IHC maturation and establishment of cochlear tonotopy (Johnson *et al.* 2013*a*). Modulation of firing activity by endogenous ATP has also been observed in the developing cochlear nucleus (CN), the first central station along the afferent auditory pathway (Dietz *et al.* 2012). Here, the neuronal excitability is attuned in a cell-specific manner, such that ATP increases action potential (AP) firing in bushy cells (BCs) but not in stellate cells (Milenkovic *et al.* 2009; Dietz *et al.* 2012). The increased excitability of BCs occurring around hearing onset is mediated by yet unidentified non-selective cation channels (P2XR), which evoke calcium transients and activate protein kinase C (PKC) (Milenkovic *et al.* 2009). Slice recordings conducted in pre-hearing gerbils (<P12) revealed that ∼90% of spherical BCs, 80% of globular BCs and 55% of principal neurons (PNs) from the medial nucleus of the trapezoid body (MNTB) are affected by ATP. From *in vivo* recordings conducted shortly after hearing onset in the rostral part of the anteroventral cochlear nucleus (AVCN; frequencies<4 kHz) or in the MNTB, it was concluded that only ∼50% of BCs and 10% of PNs were engaged with purinergic modulation (Dietz *et al.* 2012). This raised the question of whether a specific developmental mechanism may regulate the activity of central auditory neurons with respect to their tonotopic position (i.e. sound frequency selectivity). Moreover, it remained ambiguous which P2XR subtype is mediating the ATP effects in BCs.

The present study aimed to describe the tonotopic pattern of purinergic modulation during early postnatal development of the CN. In addition, temporal properties of APs in neurons affected by ATP were investigated in detail using *in vivo* juxtacellular recordings and whole-cell recordings in acute slices. Finally, by combining recordings and pharmacology *in vivo*, in slices and in human embryonic kidney 293 (HEK) cells expressing defined P2X receptors, it was determined that the heteromeric P2X2/3R mediate the observed long lasting change in intrinsic neuronal excitability.

Methods

Ethical approval

The experimental procedures were approved by the Saxonian district Government Leipzig (T 115/10, T 93/11, T 67/13 and TVV 06/09) and were conducted in agreement with regulations applying to the University of Leipzig according to the European Communities Council Directive (2010/63/EU). Mongolian gerbils (*Meriones unguiculatus*) were bred at the animal facility of the Faculty of Biosciences, Pharmacy and Psychology, University of Leipzig. Animals had *ad libitum* access to food and water and grew under a 12:12 h day/night cycle. All available measures were taken to minimize animals' pain and suffering.

In vivo experiments

Recordings were performed in 36 gerbils of either sex aged postnatal days 13–23 (P13–23) and >P60. Data were acquired shortly after hearing onset (>P12) (Woolf and Ryan, 1984) to use the acoustic responsiveness for characterization of units in the ventral cochlear nucleus

(VCN) (Rhode and Smith, 1986). We refrained from using pre-hearing animals because, in a previous attempt, it was not possible to obtain stable recordings with multibarrel electrodes over longer periods as a result of the soft consistency of the immature skull and nervous tissue in these young animals (Dietz *et al.* 2012).

Surgical preparation

For surgical preparation, animals were anaesthetized with an initial I.P. injection of a mixture of ketamine hydrochloride (0.1 mg g^{-1} body weight; Ketavet; Pfizer, New York, NY, USA) and xylazine hydrochloride (5 μg g^{-1} body weight; Rompun; Bayer, Leverkusen, Germany). Throughout the recording sessions, anaesthesia was maintained by additional S.C. application of one-third of the initial dose, every ∼90 min. Animals were fixed in the stereotaxic device by a metal bolt glued to the skull exposed around the bregma point. The recording electrode was inserted through a hole (diameter 1 mm) drilled 1 mm lateral to the midline and 1800–2000 μm caudal to the lambda suture. A second hole (diameter 0.5 mm) was located on the midline and used to position the reference electrode in the superficial cerebellum. The VCN was approached dorsally by perpendicular electrode penetrations in the animals tilted at 14–18° to the mid-sagittal plane.

Acoustic stimulation

Recordings were performed in a sound-attenuated chamber (Type 400; Industrial Acoustic Company, North Aurora, IL, USA) with the animal stabilized in a custom made stereotaxic apparatus positioned on a vibration-isolated table. Animal temperature was kept between 37 and 38 °C with a feedback-controlled heating pad. Auditory stimuli were digitally generated using custom-written Matlab software (The MathWorks Inc., Natick, MA, USA). The stimuli were transferred to a D/A converter (RP2.1 real-time processor, 97.7 kHz sampling rate; Tucker-Davis Technologies, Alachua, FL, USA), delivered through custom-made earphones (acoustic transducer: DT 770 pro; Beyer Dynamics, Heilbronn Germany) fitted with plastic tubings (length 35 mm, diameter 5 mm) and positioned into the outer ear canal at a distance of ∼4 mm to the eardrum.

Data acquisition

To reveal potential topographic differences in purinergic modulation during development, single unit recordings were performed at different positions throughout the VCN. The recording sites were referenced to the caudal pole of the posteroventral cochlear nucleus (PVCN), which was targeted by recording multi-unit activity with low impedance glass micropipettes (GB150F-10; Science Products, Hofheim, Germany; 1–5 MΩ filled with 3 M KCl). After narrowing down the target area, juxtacellular recordings were performed at defined positions along the caudal–rostral axis of the VCN by means of three- and four-barrelled piggy-back electrodes (tip diameter 5–8 μm, recording barrel protruding 15–25 μm, impedance 8–15 MΩ (GB200F-10, 3GB120F-10, 4GB120F-10; Science Products) (Havey and Caspary, 1980; Dehmel *et al.* 2010; Dietz *et al.* 2012).

Two previously described stimulation protocols were used (Dietz *et al.* 2012). (1) Pure tone pulses (100 ms duration, 5 ms rise–fall time, 100 ms interstimulus interval) were presented within a predefined matrix of frequency/intensity pairs (20 frequencies on a logarithmic scale, 10 intensity levels on a linear scale, four or five repetitions per frequency-intensity combination) to compute the excitatory response areas of extracellularly recorded single units. Acoustically excitable units were characterized by their characteristic frequency (CF) (i.e. the frequency that, at the lowest absolute intensity, caused an increase in AP spiking above the spontaneous rate). (2) Spontaneous neuronal discharge activity was assessed in the absence of acoustic stimulation to determine the average firing rate, interspike interval (ISI) probability and mean waveform of recorded signals. Recordings of spontaneous activity were carried out before, during and after the pharmacological application.

Drugs ($\alpha\beta$-meATP: 20 mM, pH 8; AF-353: 1 mM, pH 8; TNP-ATP: 1 mM, pH 8; glycine: 400 mM, pH 4) were applied iontophoretically (MVCS-02C-45; npi electronics GmbH; Tamm, Germany) with increasing current steps ($\alpha\beta$-meATP, AF-353, TNP-ATP: –50 to −150 nA; glycine +5 to +50 nA) separated by at least 60 s. The holding current for each barrel was ±20 nA. One barrel was filled with 1 M sodium acetate and served as a balancing channel to alleviate current effects.

In addition to the single unit recordings, tonotopic mapping was performed along the dorso–ventral axis of the VCN during each electrode penetration. For this purpose, CFs were acquired from multi-unit recordings at 200 μm steps and the values from multiple penetrations were used thereafter for the construction of VCN tonotopic maps. The recording sites were histologically verified by iontophoretic injection of Fluorogold (+5 μA for 5 min) in the rostral AVCN, caudal AVCN and caudal PVCN. At the end of the experiments, the fully anaesthetized animal was exposed to lethal concentration of carbon dioxide and then intracardially perfused with 0.9% NaCl solution followed by 5% paraformaldehyde. Parasagittal slices containing the CN complex were cut on a vibratome and the tissue sections (50 μm thick) were visualized under the confocal microscope (TCS PS5; Leica Microsystems, Wetzlar, Germany).

Data analysis

Recorded voltage signals were amplified (Neuroprobe 1600; A-M Systems, Carlsborg, WA, USA), bandpass filtered (0.3–7 kHz), digitized at a sampling rate of 97.7 kHz (RP2.1; Tucker-Davis Technologies) and stored for offline analysis using a custom-written Matlab software (B. Englitz, Department of Neurophysiology, University of Nijmegen, The Netherlands; C. Keine, Department of Neurobiology, University of Leipzig, Leipzig, Germany). Recordings used for quantitative analysis had to meet four criteria: (i) signal-to-noise ratio at least 8:1; (ii) fluctuations of the spike height not exceeding 20% (in average 15 $\pm$ 0.6%, $n = 36$); (iii) spontaneous AP discharges could be reversibly blocked by glycine application; and (iv) the recorded signals showed a stable, uniform waveform. BCs were identified by their complex waveform allowing a differentiation of prepotential, EPSP and AP, and by a primary-like/primary-like with notch peristimulus time histogram (Pfeiffer, 1966; Young *et al.* 1988; Blackburn and Sachs, 1989; Englitz *et al.* 2009; Typlt *et al.* 2010; Typlt *et al.* 2012). Stellate cells were characterized by their typical biphasic waveform and 'chopper' peristimulus time histogram (Rhode and Smith, 1986; Young *et al.* 1988; Typlt *et al.* 2012). Because of their narrow spatial dispersion (mostly PVCN) and the mostly weak signal-to-noise ratio, only two recordings of octopus cells were obtained and, therefore, excluded from the analysis.

It was necessary to impose the above described criteria on the recorded signals to allow for a differential analysis of the single components contained in complex waveforms. In these signals, the EPSP time point was defined by calculating the local minimum of the first derivative preceding the AP maximum. For signals in which the EPSP was temporally separated from the AP, the first local maximum preceding the AP was taken as the EPSP time point. The EPSP-AP delay was then calculated as the time between EPSP time point and the positive peak of the AP component. The AP half-width (APhw) was measured at the half-maximal AP height after the integration (anti-differentiation) of the original voltage trace. Because the juxtacellularly recorded AP is mostly proportional to the first derivative of the respective intracellular recording, this allows for quantification of temporal AP properties (Bean, 2007). Experimentally induced changes in EPSP-AP delay and APhw were quantified from the mean waveforms of the APs obtained during three distinct recording periods: 10/20 s preceding the drug application (before drug), the last 10/20 s of the drug application (drug) and 10/20 s analysed 90 s after the end of the application (post drug). For units with spontaneous firing rates>10 Hz, APs were averaged for 10 s; in units with lower spontaneous rates, recording times were averaged for 20 s. Following the application of P2XR agonists or antagonists, the cells were classified as responders or non-responders based on the changes in firing properties resulting in z-values>1.65 ($P < 0.05$) (for further description, see Statistical analysis).

Slice preparation

Acute parasagittal slices (150 μm) of the CN complex were obtained from P4–16 gerbils of either sex. The animals were killed by carbon dioxide inhalation and then decapitated according to the approval by the Saxonian district Government Leipzig (T 115/10, T 93/11, T 67/13). Slicing was performed with a vibratome (HM 650; Microm International GmbH, Walldorf, Germany) in cold (3–4°C) low-calcium artificial cerebrospinal fluid (aCSF) solution containing 125 NaCl, 2.5 KCl, 0.1 $CaCl_2$, 3 $MgCl_2$, 1.25 NaH_2PO_4, 25 $NaHCO_3$, 25 glucose, 2 sodium pyruvate, 3 myo-inositol, 0.5 ascorbic acid, continuously bubbled with 5% CO_2 and 95% O_2 (pH 7.4). Slicing solution contained less Ca^{2+} and more Mg^{2+} than the standard aCSF to avoid Ca^{2+}-dependent signalling and activation of NMDAR. After cutting in ice-cold solution, slices were incubated in the standard recording aCSF containing (in mM):125 NaCl, 2.5 KCl, 2 $CaCl_2$, 1 $MgCl_2$, 1.25 NaH_2PO_4, 25 $NaHCO_3$, 25 glucose, 2 sodium pyruvate, 3 myo-inositol, 0.5 ascorbic acid, continuously bubbled with 5% CO_2 and 95% O_2 (pH 7.4) for 30 min at 37°C to clear up the tissue surface and restore cellular processes. Thereafter, slices were stored at room temperature (RT) to prolong their usability until recording. Experiments were conducted at RT (21–23 °C), except for the current clamp recordings investigating the properties of synaptically evoked APs that were performed at 34 °C. To reveal developmental changes of purinergic responses, the data were grouped as: P4, P6–7, P10–12 (before hearing onset), P13–16 (after hearing onset).

Whole-cell recordings in acute slices

Whole-cell recordings of P2XR-mediated responses were performed as described previously (Dietz *et al.* 2012). In brief, patch pipettes were made of borosilicate glass (Science Products) with PC-10 vertical puller (Narishige, Tokyo, Japan) to have resistances of 3–5 MΩ when filled with internal solution containing (mM): 130 potassium-gluconate, 10 KCl, 1 NaCl, 0.05 $CaCl_2$, 10 Hepes, 0.1 EGTA, 5 mM phosphocreatine, 2 mMATP disodium salt and 0.3 mMGTP disodium salt (pH 7.3 with KOH). Recordings of pharmacologically isolated excitatory postsynaptic currents (EPSCs) were performed with Cs-based internal solution containing (mM): 140 $CsMeSO_3$, 20 TEA-Cl, 3.3 $MgCl_2$, 10 Hepes and 0.1 EGTA (pH 7.3 with CsOH). Biocytin (0.2%)

was supplemented for labelling of recorded neurons. All slice recordings were acquired with a Multiclamp 700B amplifier (Molecular Devices, Sunnyvale, CA, USA) in current-clamp or voltage-clamp mode. In voltage-clamp recordings, series resistance (R_s, 4–10 MΩ) was compensated by>70%. In current clamp, bridge balance and pipette capacitance neutralization were set and adjusted throughout the experiment. Recordings were made from −60 mV to resemble the resting membrane potential of bushy cells (McGinley and Oertel, 2006; Price and Trussell, 2006; Milenkovic *et al.* 2007). Voltages were corrected off-line by subtracting empirically determined junction potentials of 14 mV (potassium gluconate) and 11 mV ($CsMeSO_3$) from the holding potential (V_{hold}) (Neher 1992). Recorded signals were low-pass filtered at 2 kHz and sampled at 10 kHz. Data analysis was performed using pClamp 10 software (Molecular Devices) and Matlab based scripts. P2X receptor agonists ATPγS and $\alpha\beta$-meATP (North and Surprenant, 2000; Jarvis and Khakh, 2009; Coddou *et al.* 2011) were applied via a wider-tip patch pipette mounted on a Picospritzer (General Valve Corp., Bellevue, WA, USA). After adjusting the size of the puff with fluorescent dye ATTO 488 in the initial experiments, constant stimulation conditions were assured by controlling the pipette diameter, application pressure and duration, and distance from the cell (3 μm, 2 psi, 100 ms, 20 μm, respectively). Pressure-ejection of aCSF under the same condition evoked no response (Dietz *et al.* 2012). The blockers of glutamate (10 μM NBQX, 50 μM AP-V), $GABA_A$ and $GABA_B$ (20 μM SR95531, 3 μM CGP55845), and glycine receptors (0.5 μM strychnine) were superfused with aCSF to exclude possible effects of presynaptic P2 receptors (Watano *et al.* 2004; Kreinest *et al.* 2009).

A tungsten electrode placed at the auditory nerve (AN) root was used for a 50 Hz electrical stimulation of synaptic inputs. The excitatory inputs were pharmacologically isolated with 20 μM SR95531, 3 μM CGP55845 and 0.5 μM strychnine. Following 40 pulses used to record control APs from BCs, $\alpha\beta$-meATP was pressure applied for 100 ms along with ongoing synaptic stimulation. Under this condition, the agonist application evoked only a membrane depolarization and elicited no APs. This allowed investigation of the purinergic effects on AP dynamics at the constant firing rate controlled by synaptic stimulation (50 Hz). APhw was analysed at the half-maximal AP amplitude between the AP threshold and the AP peak. Precise parameter estimation was enabled by a lowpass interpolation between the adjacent sampling points based on the algorithm published by the Institute of Electrical and Electronics Engineers (1979). The AP threshold was determined from the first derivative of recorded events. APs were classified into control events occurring before P2XR-agonist application, APs during the agonist-evoked membrane depolarization and post-depolarization APs. The respective events were classified for each cell depending on the duration of agonist-evoked depolarization, which showed a very small variation between the cells (mean ± SEM, 1.58 ± 0.19 s, $n = 10$). The same approach was used to quantify the AP width at −40 mV. AP peak potential was measured as the maximal absolute value of the membrane potential. AP latencies were quantified as the delay of AP peaks relative to the stimulus artefacts. For each cell, analysis was based on averaged data from five to seven repetitions for each experimental condition. EPSC decay phase was fitted with mono- or bi-exponential functions based on an increase in adjusted r^2 values. The weighted τ decay was calculated as $\tau_{wd} = (A_{fast} \times \tau_{fast} + A_{slow} \times \tau_{slow})/(A_{fast} + A_{slow})$, where A_{fast} and A_{slow} are amplitudes at $t = 0$ and τ_{fast} and τ_{slow} are the fast and slow time constants, respectively. In cases of mono-exponential fits, one exponential component was set to zero.When comparing the fit of two nested models (i.e. mono-exponential and bi-exponential fit), the model with more coefficients will always create a better prediction because it contains more degrees of freedom. Therefore, r^2 values of the bi-exponential fit will exceed the ones of the mono-exponential fit, although the contribution of the second term might be minimal. Yet, the adjusted r^2 only increases if the increase is higher than expected by chance. For the present data, an increase of adjusted r^2 using the bi-exponential fit indicates that the better fit is justified by the increased number of coefficients in the model, whereas a decrease in adjusted r^2 indicates that the additionally introduced coefficients do not provide a better fit to the data than would be expected by chance (Anderson-Sprecher 1994).

Post hoc labelling of biocytin-filled neurons with Cy2-conjugated streptavidin was used for morphological characterization of recorded neurons (Milenkovic *et al.* 2009; Dietz *et al.* 2012). Images were generated with a confocal laser scanning microscope (TCSSP5; Leica Microsystems).

Receptor transfection and current measurements

To characterize the responses of P2XRs measured *in vivo* or in acute slice preparation, native receptor properties were compared with currents measured in HEK293 cells transiently expressing recombinant rat P2XRs (Coddou *et al.* 2011). HEK293 cells were routinely maintained in Dulbecco's modified Eagle's medium containing 10% (v/v) fetal bovine serum (Biofluids, Rockville, MD, USA) and 100 μg ml^{-1} gentamicin (Invitrogen, Carlsbad, USA). They were plated at a density of 500 000 cells per 35 mm culture dish. The transient transfection of homomeric P2X2R or P2X3R was conducted 24 h after plating using 2 μg of respective DNA and 5 μl of LipofectAMINE 2000 reagent (Invitrogen) in 2 ml of serum-free Opti-MEM. To obtain heteromeric P2X2/3Rs,

dishes were transfected with 2 μg of P2X3R DNA and 0.5 μg of P2X2R DNA. After 4.5 h of incubation, the transfection mixture was replaced with normal culture medium. Experiments were performed 24–48 h after transfection. Patch electrodes fabricated from borosilicate glass (1B150F-3; World Precision Instruments, Sarasota, FL, USA) using a Flaming Brown horizontal puller (P-87; Sutter Instruments, Novato, CA, USA) were heat polished to a final tip resistance of 2–4 MΩ. Electrodes were filled with a solution composed of (in mM): 142 NaCl, 1 $MgCl_2$, 10 EGTA and 10 Hepes (pH 7.35 with 10 M NaOH, 306 mosmol kg^{-1}). The bath solution contained (in mM): 142 NaCl, 3 KCl, 1 $MgCl_2$, 2 $CaCl_2$, 10 glucose and 10 Hepes (pH 7.35 with 10 M NaOH, 295–305 mosmol kg^{-1}). Whole-cell voltage-clamp recordings were conducted at RT using an Axopatch 200B amplifier (Molecular Devices). The current signals were recorded from $V_{hold} = -60$ mV, filtered at 2 kHz with a low-pass Bessel filter, and captured and stored using pClamp 9 software in conjunction with the Digidata 1322A analog-to-digital converter (Molecular Devices). ATP, $\alpha\beta$-meATP and antagonists were diluted in bath solution and applied using a rapid solution exchanger system (RSC-200; Biologic Science Instruments, Mumbai, India). Concentration–response graphs were generated by normalizing the responses evoked by a range of $\alpha\beta$-meATP concentrations to the current amplitude evoked by 100 μM ATP in the same cells. To circumvent the effects of receptor desensitization, agonists were administered with a washout interval of 1–5 min between each application, unless another experimental protocol was required. Each experiment was repeated in at least four separate cells and each data point was obtained from more than three applications in a single cell.

Statistical analysis

Data sets were tested for Gaussian distribution prior to comparison using Student's *t* test or ANOVA followed by pairwise multiple comparisons (Holm–Sidak *post hoc* test; Sigma Plot, version 11; Systat Software Inc., Chicago, IL, USA). In the case of a non-Gaussian distribution, non-parametric tests were applied, such as the Mann–Whitney ranksum test or ANOVA on ranks. Significant effects of drugs in individual cells were determined by a *z* test, with $z > 1.65$ corresponding to $P < 0.05$ and $z > 3.3$ corresponding to $P < 0.001$. One- or two-way repeated measures (RM) ANOVA was applied when appropriate to test for the effects of drugs (i.e. before-drug, drug and after-drug conditions for the group of cells). Mean cumulative distributions of ISIs before and during the drug application were compared using the two-sample Kolmogorov–Smirnov test. Percentage values of responding cells were compared by a chi-squared test. In some cases, dots representing single cells are added to the box-plots to illustrate data distribution. Average data are reported as the mean ± SEM or median with 25 and 75 percentiles, depending on their distribution.

Results

Endogenous ATP shapes the AP waveform and increases firing in a subset of bushy cells

To determine the effects of ATP signalling on the AP properties *in vivo*, extracellular single unit recordings were conducted in combination with pharmacological blockade of P2X3R or P2X2/3R with a selective antagonist AF-353 (Gever *et al.* 2006), using multibarrel piggyback electrodes (Fig. 1). Recordings were conducted in three areas of the VCN, aiming to assess the responsiveness in neurons with different characteristic frequencies along the tonotopic axis (Fig. 1*A*). The administration of AF-353 caused a sustained but reversible reduction of spiking (Fig. 1*B*). In seven out of 13 BCs tested from P13–16, the average spontaneous AP frequency was reduced to 53.4 ± 6.2% of the initial rate (Fig. 1*C*). These cells were classified as responders. The mean AP rate during a 90 s period prior to AF-353 application was 20.2 ± 3.0 AP/s; during application, it reduced to 9.4 ± 1.8 AP/s, and increased again in a 90 speriod after application to 19.9 ± 2.1 AP/s ($n = 7$, $P < 0.001$, RM ANOVA). The analysis of ISIs before and during AF-353 application revealed that blocking of P2X3R or P2X2/3R shifted the cumulative distribution plot towards longer ISIs ($P < 0.001$, Kolmogorov–Smirnov test) (Fig. 1*D*). Six of the recorded BCs did not show significant reduction of AP discharge rate, indicating insufficient expression or an absence of functional P2 receptors (AP rate before, during and following AF-353: 20.8 ± 2.8 AP/s; 21.4 ± 3.1 AP/s; 20.4 ± 3.0 AP/s; $n = 6$, $P = 0.55$, RM ANOVA). Such cells were classified as non-responders. In each cell, the functionality of the piggyback electrode had been tested beforehand by completely blocking the spiking through administration of glycine.

In slice recordings from BCs, it has been shown that extracellular ATP evokes inward current and Ca^{2+} transient (Milenkovic *et al.* 2009) gated through P2XR that generally show high Ca^{2+}-permeability (Virginio *et al.* 1998; North, 2002). Therefore, we investigated whether such signalling by the endogenous ATP may affect the AP generation and AP duration. Separate *in vivo* applications of AF-353 or TNP-ATP (P2X3R and P2X2/3R antagonists) prolonged the EPSP-AP transition time in responder cells (mean ± SEM EPSP-AP delay before, during and after AF-353: 209 ± 22 μs, 279 ± 17 μs, 224 ± 20 μs; $n = 7$, $P < 0.001$; mean ± SEM EPSP-AP delay before, during and after TNP-ATP: 228 ± 20 μs, 300 ± 21 μs, 234 ± 19 μs; $n = 8$, $P < 0.001$; two-way RM ANOVA). Because the effects of the two antagonists were comparable (EPSP-AP prolongation induced by:

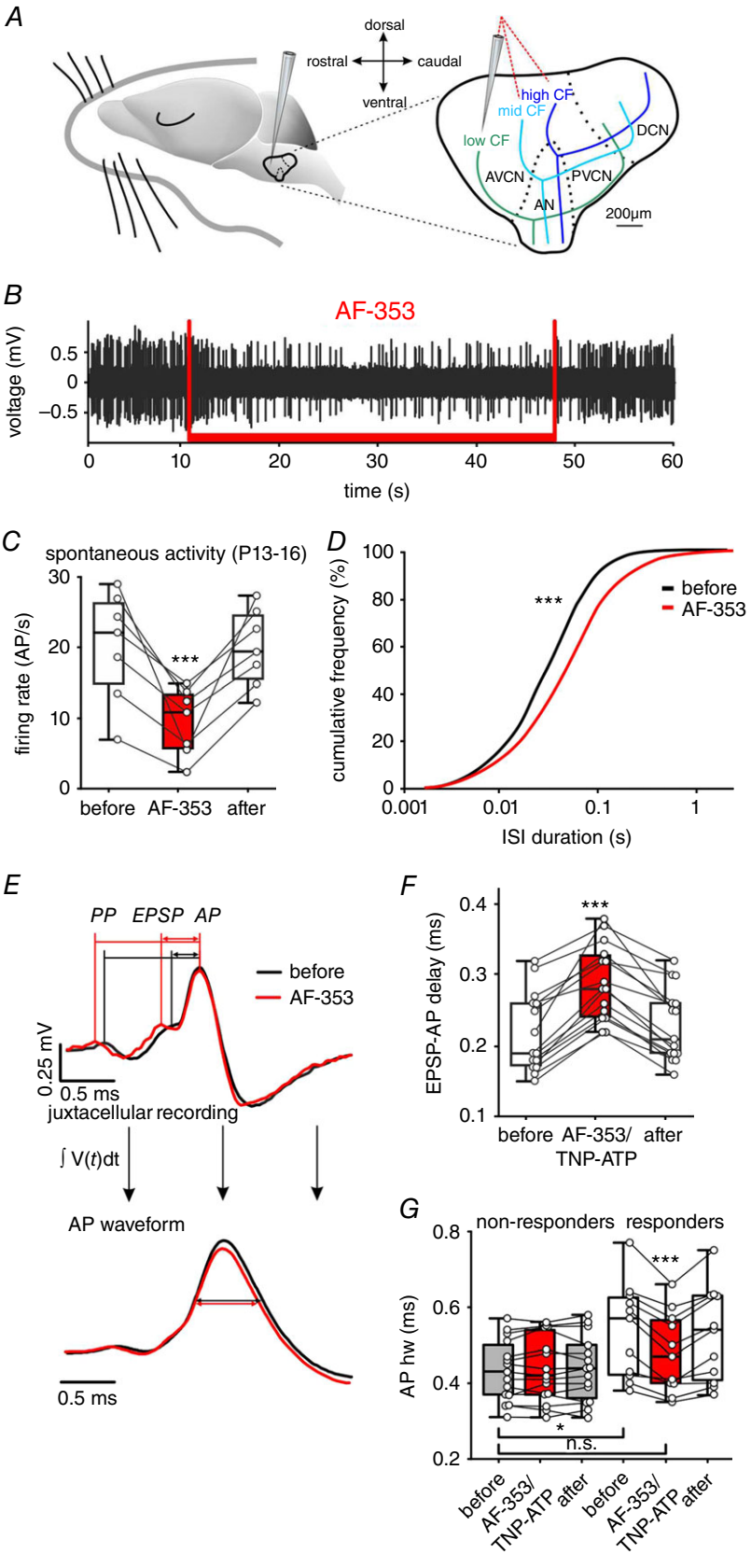

Figure 1. Endogenous activation of P2X3R or P2X2/3R contributes to *in vivo* firing activity of bushy cells from P13–16
A, schematic drawing of the parasaggital view to the CN complex with gross representations of characteristic frequencies of neurons. Note the dorso-caudal to rostro-ventral high-to-low tonotopic axis. Red dashed lines show recording electrode trajectories targeting different positions within the CN. *B*, trace of juxtacellularly recorded APs shows a reduction of firing rate during the application of the P2X3R and P2X2/3R antagonist AF-353 (1 mM; red bar). *C*, summary of the reversible AF-353 inhibition of spontaneous firing in seven BCs (circles); box-plots show medians, the 25 and 75 percentiles, and the interdecile ranges (***$P < 0.001$, RM ANOVA). *D*, cumulative distribution of ISIs for the same seven cells before (black) and during (red), AF-353 application (***$P < 0.001$, Kolmogorov–Smirnov test). *E*, top: mean waveforms of 245 juxtacellularly recorded APs under control condition (black) and of 141 APs during AF-353 application (red). The wave forms are aligned at the peak of APs. Note that AF-353 application prolongs the EPSP-AP transition time but not the PP-EPSP time. Bottom: integral of the mean AP waveforms of the signals shown above. Horizontal lines show the narrower APhw during AF-353 application. *F*, summary data showing a reversible prolongation of EPSP-AP transition time as an effect of P2X3R or P2X2/3R antagonists AF-353 or TNP-ATP (***$P < 0.001$, RM ANOVA). *G*, in BCs showing reduction of spontaneous AP firing upon AF-353 or TNP-ATP (responders), the application also caused a reversible reduction of APhw (white/red box-plots; ***$P < 0.001$, two-way ANOVA). Prior to antagonist application, the APhw in responder cells was longer than in non-responder cells (white *vs.* grey box-plots, *$P < 0.05$, two-way ANOVA). Note the similar APhw values between the responder cells under antagonist and non-responder cells (red responder *vs.* grey box-plots). [Colour figure can be viewed at wileyonlinelibrary.com]

AF-353 = 37.2 ± 6.7%, TNP-ATP = 34 ± 6.7%, $P = 0.75$, *t* test), data were pooled together [median EPSP-AP delay before, during and after the antagonist: 190 μs (173; 260), 280 μs (242; 328), 210 μs (190; 260); $n = 15$, $P < 0.001$, RM ANOVA on ranks] (Fig. 1*E* and *F*). Notably, the waveform analysis consistently showed that all APs were preceded by presynaptic action potentials (PPs), before and during the antagonist application ($n = 3236$, $n = 1531$ from 12 cells, respectively). This result suggests that the endogenous ATP facilitates presynaptic to postsynaptic coupling, rather than evoking APs *per se*.

To assess the modulatory ATP effect on AP duration, the extracellularly recorded signals were integrated to obtain the AP waveform from which then the AP width was quantified (Bean, 2007). The mean waveforms showed a longer APhw during the endogenous activation of P2X3 or P2X2/3R (mean ± SEM APhw before, during and after the antagonist: 538 ± 38 μs, 479 ± 32 μs, 526 ± 37 μs; $n = 11$, $P < 0.001$, two-way RM ANOVA). Notably, the faster APs generated in the presence of P2X3R or P2X2/3R antagonists in responder cells were comparable to APs in non-responder BCs (mean ± SEM APhw of responders + antagonist *vs.* non-responders: 479 ± 32μs, $n = 11$ *vs.* 433 ± 21 μs, $n = 15$; $P = 0.21$) (Fig. 1*G*). In non-responders, the administration of antagonists had no effect (mean ± SEM APhw before, during and after antagonist: 433 ± 21 μs, 438 ± 22 μs, 437 ± 22 μs; $n = 15$; $P = 0.0.49$, two-way RM ANOVA). Taken together, these data suggest that, in a subset of BCs from P13–16, ATP has a dual effect: (i) facilitation of AP generation by shortening EPSP-AP time and (ii) prolongation of APs.

Stellate cells did not change the firing rate upon exposure to AF-353 or TNP-ATP (mean ± SEM AP rate before, during and after the administration of the antagonists: 18.0 ± 6.7 AP/s, 17.6 ± 6.4 AP/s, 17.1 ± 6.3 AP/s, $n = 9$, $P = 0.19$, RM ANOVA) (data not shown). Also, the antagonists did not affect their APhw (mean ± SEM APhw before, during and after the antagonist: 335 ± 17 μs, 340 ± 18 μs, 343 ± 18 μs; $n = 9$, $P = 0.22$, RM ANOVA). In comparison with both responder and non-responder BCs, stellate cells have a shorter APhw ($P < 0.001$, ANOVA on ranks). Thus, the generally longer APs in BCs in responder neurons can be additionally prolonged by endogenous ATP.

P2XRs on bushy cells resemble mixed P2X2 and P2X3 characteristics

To evaluate the effects of P2X3R or P2X2/3R observed *in vivo*, whole-cell recordings were acquired from BCs in acute brainstem slices. The morphology of recorded cells, as revealed by a *post hoc* biocytin labelling (Fig. 2*A*, left), resembled the characteristics of large BCs: oval cell soma, developing dendritic tree and the axon passing along the

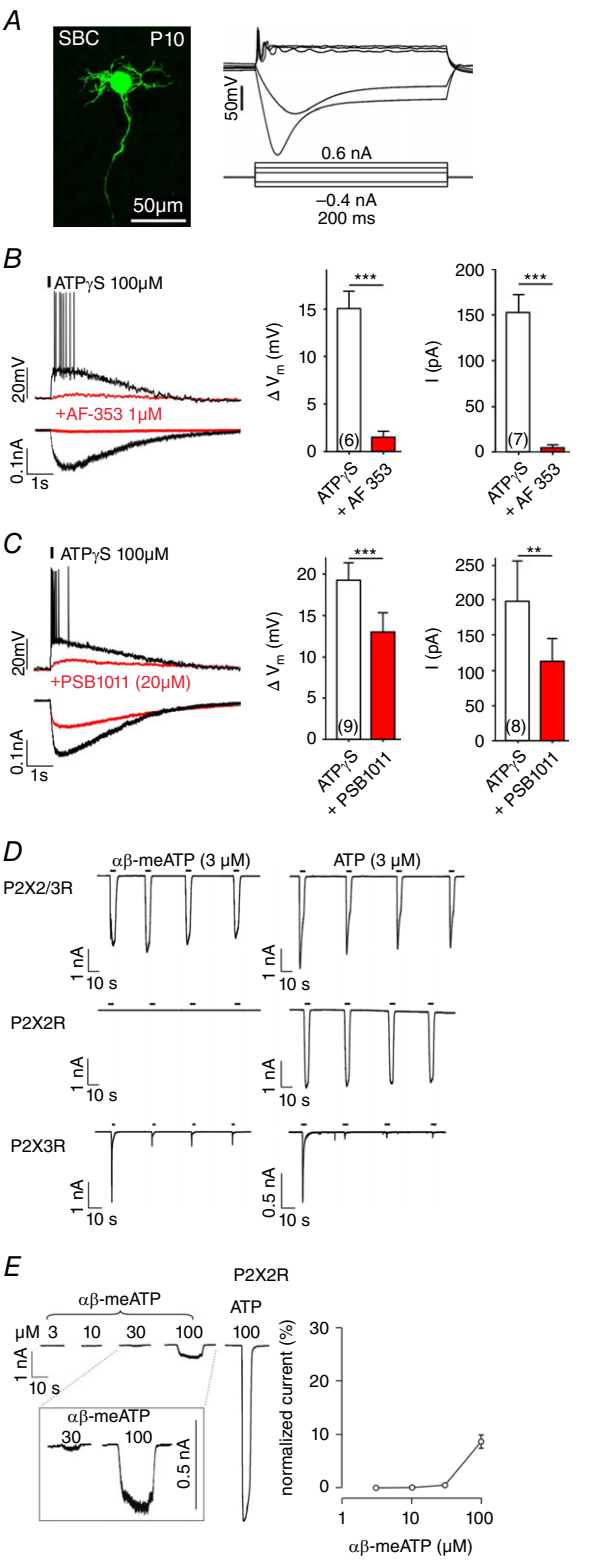

Figure 2. Characterization of the native P2XR by comparison of responses in bushy cells and in HEK293 cells expressing homomeric P2X2R, P2X3R and heteromeric P2X2/3R
A, BCs from P10–12 were characterized by the *post hoc* labelling of biocytin-filled neurons (left), phasic firing after supra-threshold depolarization, and the prominent sag after hyperpolarizing current

ventral acoustic stria (Rouiller and Ryugo, 1984; Hackney *et al.* 1990; Morest *et al.* 1990; Ryugo and Sento, 1991; Ostapoff *et al.* 1994). Voltage responses to current steps were also typical for large BCs (Fig. 2*A*, right) (i.e. a single or few APs at the onset of positive suprathreshold pulses, and hyperpolarization sagging back toward rest as a result of prominent Ih conductance activated by negative pulses (Francis and Manis, 2000; Leao *et al.* 2005; Cao *et al.* 2007; Milenkovic *et al.* 2009). In agreement with our previous studies (Milenkovic *et al.* 2009, Dietz *et al.* 2012), application of ATPγS (100 μM, 150 ms) evoked membrane depolarization lasting for several seconds with the APs transiently riding on top of this depolarization (Fig. 2*B*, left). In voltage clamp, the same application induced a fast non-desensitizing inward current that temporally matched the membrane potential change. Superfusion of AF-353 (1 μM) efficiently blocked the ATPγS-induced membrane depolarization by 90% ($n = 6$, $P < 0.001$, paired t test) and the whole-cell current by 99% ($n = 7$, $P < 0.001$, paired t test) (Fig. 2*B*, right). These data corroborate our observation from *in vivo* recordings suggesting that the modulatory effects are mediated by receptors containing P2X3/P2X2/3 subunits.

To address the possibility that homomeric P2X2R mediate the effects, a potent and selective P2X2 receptor antagonist PSB1011 (Baqi *et al.* 2011) was applied at increasing concentrations of 5, 10 and 20 μM. Even at the highest concentration, the ATPγS-evoked responses were inhibited by less than 43% (mean ± SEM ATPγS-induced depolarization = 19.2 ± 2.2 mV, ATPγS + PSB1011 = 12.8 ± 2.4 mV, $n = 9$, $P < 0.001$, paired t test; mean ± SEM ATPγS-induced current = 197.1 ± 59.4 pA, ATPγS + PSB1011 = 112.3 ± 32.8 pA, $n = 8$, $P = 0.006$, paired t test] (Fig. 2*C*). These results suggest that purinergic modulation of BCs is only partially mediated by P2X2R receptor subunits. Taken together, our data are consistent with a P2X receptor type featuring mixed P2X2R and P2X3R characteristics.

steps (right). *B*, left: voltage and current responses of the cell shown in (*A*) to a puff application of ATPγS (150 ms, 2 psi, 20 μm from cell soma), before (black) and after superfusion of AF-353 (red). The responses were evoked from $V_h = -60$ mV. Right: summary data for the inhibitory effect of AF-353 on the ATPγS-induced membrane depolarization and current. *C*, limited inhibitory potency of the P2X2 antagonist PSB1011. Even at the PSB1011 concentration of 20 μM, the responses to ATPγS were only partially inhibited (**$P < 0.01$, ***$P < 0.001$, paired t test). Cell numbers are given in parentheses. *D*, whole-cell current responses during repetitive agonist applications in HEK293 cells co-expressing P2X2R and P2X3R (top row), P2X2R (middle row) or P2X3R (bottom row). Cells were stimulated for 5 s with 3 μM $\alpha\beta$-meATP (left column) or 3 μM ATP (right column). Note that the P2X2R did not respond to 3 μM $\alpha\beta$-meATP, whereas the P2X3R current highly desensitized after the first application of $\alpha\beta$-meATP or ATP. This indicates that agonist-induced currents in cells co-expressing P2X2R and P2X3R were gated by P2X2/3R heteromers. *E*, concentration-dependent effects of $\alpha\beta$-meATP show a threshold concentration of 30 μM for activation of P2X2R. Left: representative traces obtained from the same cell stimulated with increasing agonist concentrations for 10 s. The last recording shows the response to 100 μM ATP. Inset: magnification of currents gated by 30 and 100 μM $\alpha\beta$-meATP. Right: currents elicited by $\alpha\beta$-meATP were normalized against the response evoked by 100 μM ATP (mean ± SEM, $n = 4$). [Colour figure can be viewed at wileyonlinelibrary.com]

Characterization of the native P2XR type

Characterization of the native P2 receptors is generally hampered by the lack of highly specific agonists and antagonists (Gever *et al.* 2006). It was important to pinpoint the receptors mediating modulation to assess the potential effects on development of auditory brainstem circuits both in the present study, as well as in future studies using genetically modified mice. To provide a comprehensive understanding of P2XR responses in slice recordings, pharmacological characterization was performed in controlled P2X2R, P2X3R and P2X2/3R-expression systems, which allowed a *posthoc* comparison of the effects. In general, HEK293 cells transfected with P2X2R and P2X3R cDNA express homomeric P2X2R and P2X3R, as well as heteromeric P2X2/3R. To discriminate between these three populations of receptors expressed in the same cell, we designed an experimental protocol with repetitive agonist stimulations. Figure 2*D* shows representative recordings of three different cells, expressing either the P2X2/3R receptors, P2X2R only or P2X3R only. Cells were stimulated repetitively for 5 s with $\alpha\beta$-meATP or ATP, using a rapid solution exchanger system. Repetitive applications of $\alpha\beta$-meATP or ATP elicited stable, non-desensitizing currents only in cells expressing P2X2/3R. The P2X2R were not activated by $\alpha\beta$-meATP, whereas ATP induced robust and reproducible currents. On the other hand, P2X3R were activated by both $\alpha\beta$-meATP and ATP during the initial agonist application. During subsequent stimulations, P2X3R remained mostly inactive, indicating a strong desensitization after the first activation.

In agreement with a previous study (Lewis *et al.* 1995), these results demonstrate that the most distinctive feature of the P2X2/3R is a non-desensitizing current (P2X2R phenotype) elicited by the P2X3R-preferring agonist $\alpha\beta$-meATP. Next, the concentration dependency of homomeric P2X2Rs was quantified through successive stimulations of the same cell with increasing $\alpha\beta$-meATP concentrations. Figure 2*E* shows the lack of response to 3 and 10 μM $\alpha\beta$-meATP, a threshold-like response to 30 μM $\alpha\beta$-meATP and a substantial current response during application of 100 μM $\alpha\beta$-meATP. Still, the amplitude of the current evoked by 100 μM $\alpha\beta$-meATP was only 10 % of the current induced by 100 μM ATP. Thus,

$\alpha\beta$-meATP is a partial and low affinity agonist for P2X2R, whereas, at concentrations up to 10 μM, it could be used as a selective P2X2/3R agonist when applied repetitively.

The HEK293 cell system was also used to test the potency of AF-353 in inhibiting currents gated by P2X2/3R. Co-application of the antagonist with $\alpha\beta$-meATP caused a weak but significant reduction of the current. Almost complete inhibition was observed after a 30 s antagonist pre-application followed by co-application (Fig. 3*A* and *B*). The inhibitory potency of AF-353 developed slowly over time and showed prolonged effect on P2X2/3R during the washout period (Fig. 3*A* and *C*). Subsequently, the AF-353 inhibition of P2X2/3R, P2X3R and P2X2R currents was compared (Fig. 3*D*). Following a 30 s pre-application of AF-353, the cells were stimulated for 5 s with 3 μM $\alpha\beta$-meATP (P2X2/3R and P2X3R) or 10 μM ATP (P2X2R) along with ongoing antagonist treatment. Pauses of 10 min were introduced between successive stimuli to allow for recovery from desensitization. Under these experimental conditions, AF-353 blocked both P2X2/3R and P2X3R currents, whereas the P2X2R current was not affected. The specificity of AF-353 in blocking P2X3R or P2X2/3R was further demonstrated in P2X2R-expressing cells, where the currents elicited by 100 μM $\alpha\beta$-meATP were insensitive to 1 μM AF-353 (Fig. 3*E*). Thus, our data are consistent with the previous study reporting high selectivity of AF-353 for P2X2/3R and P2X3R but no inhibitory effect on P2X2R (Gever *et al.* 2006).

Preiously, we showed the strong potency of TNP-ATP to inhibit purinergic responses of BCs *in vivo* and in acute slices (Dietz *et al.* 2012). To determine the potential receptor type inhibited by TNP-ATP, its effects were tested on P2X2/3R, P2X3R and P2X2R. In cells with heteromeric P2X2/3Rs, co-application of TNP-ATP with $\alpha\beta$-meATP, as well as combined pre- and co-application, completely inhibited the membrane current (Fig. 3*F* and *G*). By contrast to AF-353, TNP-ATP also inhibited P2X2R-mediated currents by 40%, when it was co-applied with ATP (Fig. 3*H* and *I*). Compared to AF-353 that specifically blocks P2X2/3R and P2X3R, TNP-ATP showed lesser selectivity by also inhibiting P2X2R. Yet the effect on P2X2/3R and P2X3R currents was much stronger compared to P2X2R. Taken together, these results suggest that AF-353 or TNP-ATP in combination with $\alpha\beta$-meATP can be used as a suitable pharmacological tool for investigating P2X2/3R.

P2X2/3Rs tune the APs in developing bushy cells

After confirming the high selectivity of $\alpha\beta$-meATP for P2X2/3R and P2X3R in transfected HEK293 cells, we investigated the functional role of the respective receptors *in vivo* and in slice experiments. Consistent with the data in Fig. 1, *in vivo* recordings in P13–16 animals with agonist applications revealed two groups of bushy cells: non-responders (9/19) (i.e. units that did not change the AP discharge rate under $\alpha\beta$-meATP; mean $\pm$ SEM AP frequency during 90 s prior to $\alpha\beta$-meATP $=$ 19.7 $\pm$ 4.5 AP/s, AP frequency during $\alpha\beta$-meATP $=$ 20 $\pm$ 4.5 AP/s, AP frequency during 90 s following $\alpha\beta$-meATP $=$ 19.7 $\pm$ 4.4 AP/s, $n = 9$, $P = 0.54$, RM ANOVA) and responders (10/19) (i.e. BCs that significantly increased the spontaneous firing ($z > 1.65$) during the application; mean $\pm$ SEM application duration $=$ 35.2 $\pm$ 1.7 s, $n = 10$) (Fig. 4*A* and *B*) [median AP frequency during 90 s prior to $\alpha\beta$-meATP $=$ 15.4 AP/s (6.1; 20.5), AP frequency during $\alpha\beta$-meATP $=$ 20 AP/s (7.7; 25.9), AP frequency during 90 s following $\alpha\beta$-meATP $=$ 16.2 AP/s (7.2; 19), $n = 10$, $P = 0.008$, RM ANOVA on ranks]. A comparable increase in firing was observed during the first and the last 10 s of application, indicating the lack of receptor desensitization (18.7 $\pm$ 3.5 AP/s and 18.9 $\pm$ 4 AP/s, respectively; $n = 10$, $P = 0.8$, paired t test). During increased firing, no isolated APs (i.e. lacking a preceding PP) were observed, suggesting that $\alpha\beta$-meATP is not evoking APs *per se* ($n = 1627$, $n = 7$), but rather raising the probability of AP generation in response to the endbulb of Held input.

To confirm that the endogenous ATP release attunes the APs through P2X2/3R-activation, as suggested by the data in Fig. 1, the effects of $\alpha\beta$-meATP on AP generation and duration were assessed. Administration of $\alpha\beta$-meATP most prominently increased the incidence of APs at ISIs 10–100 ms ($P < 0.001$, Kolmogorov–Smirnov test) (Fig. 4*C*). The EPSP-AP transition time was shorter during the agonist application (Fig. 4*D* and *E*) (mean $\pm$ SEM EPSP-AP delay before, during and after the application: 209 $\pm$ 13 μs, 196 $\pm$ 16 μs, 213 $\pm$ 13 μs; $n = 10$, $P = 0.013$, RM ANOVA). Furthermore, in responder cells, the agonist also prolonged the APhw (Fig. 4*D* and *F*) (mean $\pm$ SEM APhw before, during and after $\alpha\beta$-meATP: 541 $\pm$ 34 μs, 581 $\pm$ 38 μs, 555 $\pm$ 38 μs; $n = 10$, $P = 0.003$, two-way RM ANOVA). Under the control condition, the APhw in responder cells is conspicuously longer than in non-responders (Fig. 4*F*) (responders *vs.* non-responders: 541 $\pm$ 34 μs, $n = 10$; 434 $\pm$ 20 μs, $n = 9$; $P = 0.02$, two-way RM ANOVA with Holm–Sidak *post hoc* test). In the latter, the APhw did not change during the agonist administration (mean $\pm$ SEM APhw before, during and after $\alpha\beta$-meATP: 434 $\pm$ 20 μs, 438 $\pm$ 20 μs, 443 $\pm$ 21 μs; $n = 9$, $P = 0.14$, two-way RM ANOVA). Taken together, these data demonstrate that in a population of BCs from P13–16 gerbils, the endogenous P2X2/3R activation facilitates the AP generation and prolongs the APs. In these cells, the respective effects can be augmented through additional receptor activation with an exogenous agonist.

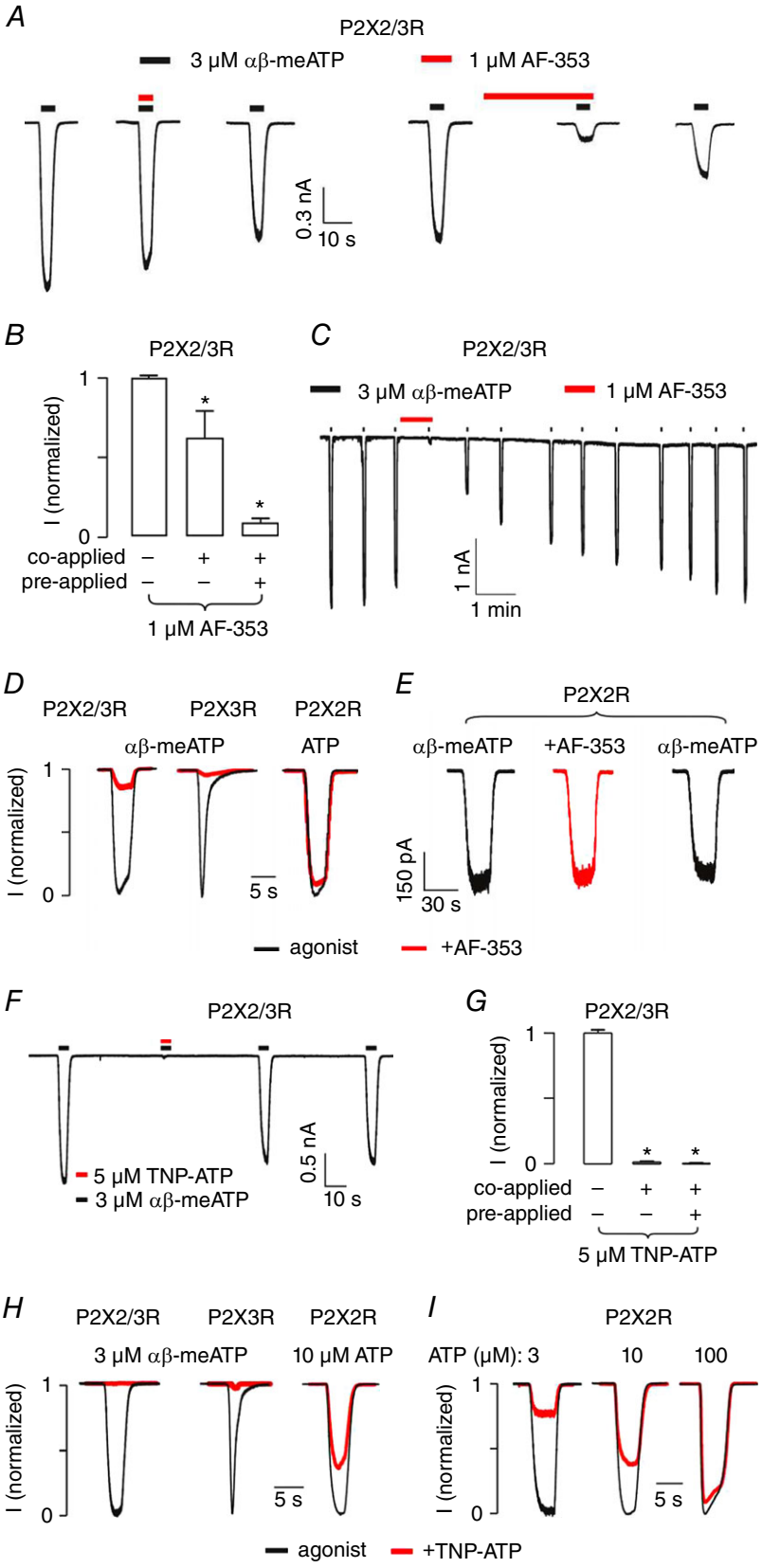

Figure 3. Receptor-specific effects of AF-353 and TNP-ATP on P2XR currents
A, representative recordings from a HEK293 cell co-expressing P2X2 and P2X3R during the second, third and fourth (both panels: left, middle and right, respectively) application of 3 μM $\alpha\beta$-meATP. In addition, 1 μM AF-353 (red) was either co-applied (left panel: middle) or pre- and co-applied (right panel: middle) with the agonist. *B*, summary of the inhibition induced by 1 μM AF-353 shows higher effectiveness after pre-application. *C*, slow washout of 1 μM AF-353 (red) after pre-application for 30 s and co-application with 3 μM $\alpha\beta$-meATP. *D*, selectivity of AF-353. Black traces represent the responses evoked by 3 μM $\alpha\beta$-meATP (P2X2/3R and P2X3R) or by 10 μM ATP (P2X2R). Red traces depict current responses from the same cells in the presence of 1 μM AF-353. AF-353 was pre-applied for 30 s and then co-applied with agonist. *E*, lack of AF-353 effect on P2X2R-mediated currents gated by 100 μM $\alpha\beta$-meATP. Traces shown are from the same cell during the first (left), second (middle) and third (right) application, with 1 μM AF-353 pre-applied for 30 s and then co-applied with agonist during its second application. In all experiments, duration of agonist application was 5 s. *F*, representative recordings from a cell co-expressing P2X2R and P2X3R stimulated with 3 μM $\alpha\beta$-meATP for 5 s (black). Co-application of TNP-ATP (5 μM, red) completely inhibited the current. Beforehand, $\alpha\beta$-meATP had been applied to desensitize P2X3R-mediated responses (not shown). *G*, summary of the inhibition induced by 5 μM TNP-ATP on P2X2/3R. *H*, selectivity of TNP-ATP. Black traces represent the responses evoked by 3 μM $\alpha\beta$-meATP (P2X2/3R and P2X3R) or 10 μM ATP (P2X2R) and red traces the current responses from the same cells in the presence of 5 μM TNP-ATP. Duration of agonist application was 5 s and TNP-ATP was co-applied with agonist. *I*, competitive antagonistic effect of TNP-ATP on ATP-induced P2X2R currents. Normalized currents gated by 3 (left), 10 (middle) or 100 μM (right) ATP (for 5 s) in the absence (black) or in the presence (red) of 5 μM TNP-ATP. [Colour figure can be viewed at wileyonlinelibrary.com]

Long-lasting modulation of the temporal AP properties

To exclude the possibility that the prolonged APs observed *in vivo* are a consequence of increased firing rates caused by the P2X2/3R agonist, we performed slice recordings allowing for synaptic stimulation of the excitatory input at constant rates (Fig. 5). Initially, BCs were classified into responders and non-responders based on significant effects of $\alpha\beta$-meATP on the V_m, measured in current clamp ($z > 3.3$ in 10 out of 12 cells from P10, mean ± SEM $\alpha\beta$-meATP-evoked depolarization in responders = 10 ± 0.8 mV, $n = 10$). Under the control condition (without $\alpha\beta$-meATP), the APhw quantified from the last 10 APs in a 50 pulse train did not depend on the input frequency (APhw at 34 °C: 20 Hz = 0.63 ± 0.04 ms, 50 Hz = 0.63 ± 0.04 ms, $n = 10$, $P = 0.99$, paired t test). Stimulation frequency of 20 Hz was used to mimic the average *in vivo* spontaneous rate of BCs at P13–16 (19 ± 2 AP/s, $n = 32$). A higher stimulation rate of 50 Hz resembles the average firing frequency within a burst in BCs at P9 (45 ± 3.4 AP/s,

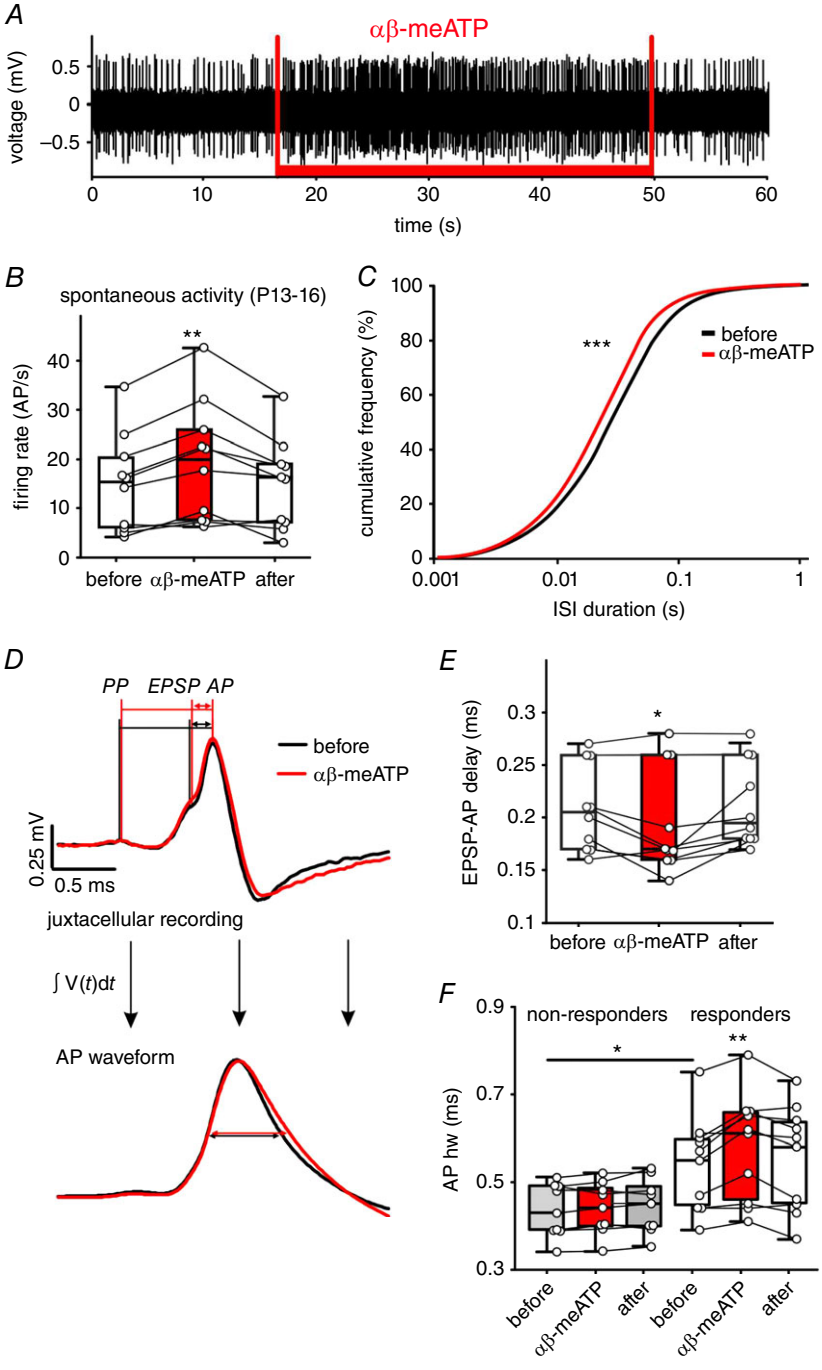

Figure 4. Effects of P2X2/3R activation on APs *in vivo*
A, juxtacellular recording showing a persistent increase in AP frequency during iontophoretic application of $\alpha\beta$-meATP (20 mM, red bar). *B*, changes in spontaneous spiking evoked by $\alpha\beta$-meATP in 10 BCs and calculated as average firing rate before, during and after drug application. Circles depict individual cells; box-plots depict the medians, 25 and 75 percentiles, and the interdeciles (**$P < 0.01$, RM ANOVA). *C*, ISIs for 10 BCs before (black) and during (red) $\alpha\beta$-meATP administration shown as cumulative distribution (***$P < 0.001$, Kolmogorov–Smirnov test). *D*, top: mean waveforms from 152 APs before (black) and 232 APs under the $\alpha\beta$-meATP application (red). Bottom: integrals of AP waveforms from the upper graph. Horizontal lines show the APhw. *E*, summary data showing a shorter EPSP-AP transition time caused by $\alpha\beta$-meATP (*$P < 0.05$, RM ANOVA). *F*, cells not responding to $\alpha\beta$-meATP (non-responders) have shorter APhw compared to responder cells (grey *vs*. white box-plots) (*$P < 0.05$, two-way ANOVA). In responder cells, the APhw is further prolonged by $\alpha\beta$-meATP (red box-plot) (*$P < 0.01$, two-way ANOVA). [Colour figure can be viewed at wileyonlinelibrary.com]

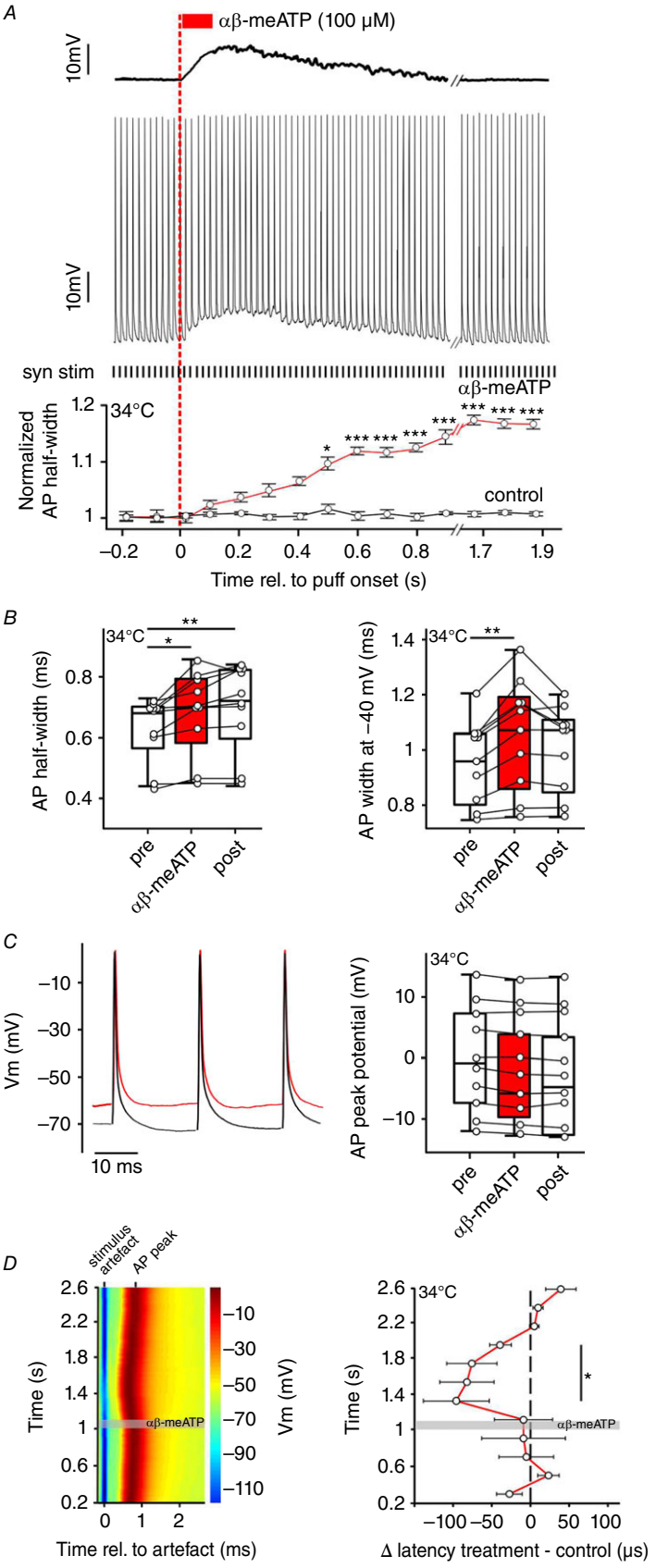

Figure 5. P2X2/3R activation affects temporal properties of APs
A, top: representative voltage trace showing BC depolarization in response to puff application of $\alpha\beta$-meATP (red bar). Dashed red line indicates the application onset. Middle: simultaneous acquisition of synaptically evoked APs in the same cell by electrical stimulation of the auditory nerve input (50 Hz, black ticks below; syn stim). Bottom: persistent prolongation of APhw reached significance after 0.45 s (red line; $^{*}P < 0.05$, $^{***}P < 0.001$, *z* test). The black line shows normalized APhw of control events, without $\alpha\beta$-meATP application. Each circle represents an average half-width for five consecutive APs. *B*, APhw (left) and the AP width at −40 mV (right) are increased upon application of $\alpha\beta$-meATP. Box-plots show medians with 25 and 75 percentiles, and interdeciles for the periods before (pre), during ($\alpha\beta$-meATP) and after (post) application ($^{*}P < 0.05$, $^{**}P < 0.01$, RM ANOVA). *C*, left: overlay of APs elicited before (0.86–0.92 s, black) and after the onset of $\alpha\beta$-meATP application (1.18–1.24 s, red). Right: membrane potential at the peak of AP ($n = 10$, $P = 0.12$, one-way RM ANOVA). *D*, left: latency changes of APs synaptically evoked at 50 Hz stimulation frequency. The responses were aligned at the stimulus artefact (blue) and the grey area depicts the duration of application. Membrane potential values are colour coded. Note the shorter AP latencies after the $\alpha\beta$-meATP application. Right: population data showing a long-lasting decrease in AP latency following the application of $\alpha\beta$-meATP (circles, red line) compared to control (black dashed line). Circles indicate average latency differences between treatment and control for 10 consecutive APs. Note the significant shortening of latencies during the time window 200–800 ms after the $\alpha\beta$-meATP application ($n = 9$, mean ± SEM, one sample *t* test). [Colour figure can be viewed at wileyonlinelibrary.com]

$n = 45$). Puff application was set to 100 ms to avoid suprathreshold depolarization and generation of APs by $\alpha\beta$-meATP. Under these conditions, the depolarization still lasted ∼15 times longer than the agonist application (mean ± SEM 1.58 ± 0.19 s, $n = 10$) (Fig. 5*A*, top). In the next step, puff application of $\alpha\beta$-meATP was combined with 50 Hz synaptic stimulation (Fig. 5*A*, middle). The application of $\alpha\beta$-meATP did not evoke additional APs, although it sustainably increased the APhw of synaptically evoked discharges (Fig. 5*A*, bottom). Figure 5*B* shows the changes in AP duration caused by $\alpha\beta$-meATP at 50 Hz firing frequency [APhw: pre (average for 0.8 s) = 0.63 ± 0.04 ms, $\alpha\beta$-meATP (average for 1.58 ± 0.19 s) = 0.68 ± 0.05 ms, post (average for 1.3 ± 0.2 s post-depolarization) = 0.69 ± 0.05; $n = 10$, $P = 0.004$, RM ANOVA]. Similar AP prolongation was observed at 20 Hz stimulation frequency, suggesting that $\alpha\beta$-meATP effect does not depend on firing frequency [APhw: pre (average for 0.8 s) = 0.63 ± 0.05 ms, $\alpha\beta$-meATP (average for 1.58 ± 0.19 s) = 0.67 ± 0.04 ms, post (average for 1.3 ± 0.2 s post-depolarization) = 0.68 ± 0.06; $n = 10$, $P = 0.009$, RM ANOVA]. APs riding on top of $\alpha\beta$-meATP-induced membrane depolarization have smaller amplitudes than those of control recordings. Still, the AP width analysis at −40 mV, aiming to exclude a potential influence of the different AP amplitudes, confirmed the effect of $\alpha\beta$-meATP [AP width at −40 mV: pre = 0.95 ± 0.05 ms, $\alpha\beta$-meATP = 1.05 ± 0.07 ms, post = 1 ± 0.05 ms; $n = 10$, $P < 0.001$, RM ANOVA] (Fig. 5*B*, right). The peak membrane potential of APs did not change under $\alpha\beta$-meATP (Fig. 5*C*) (mean ± SEM AP peak: pre = −0.16 ± 2.8 mV, $\alpha\beta$-meATP = −6.4 ± 2.9 mV, post = −4.3 ± 3.1 mV; $n = 10$, $P = 0.12$, RM ANOVA). Next, we tested the possibility that the observed AP prolongation may be caused by the mere membrane depolarization induced by $\alpha\beta$-meATP. BCs from P10 were depolarized with current injection by 14.3 ± 2.9 mV ($n = 6$) to mimic the depolarizing effect of $\alpha\beta$-meATP. The APs were evoked by simultaneous synaptic stimulation at 50 Hz (data not shown). In this case, the APhw = 0.64 ± 0.4 mV was similar to control (control *vs.* current injection, $n = 10$ and $n = 6$, respectively, $P = 0.52$, *t* test). On the other hand, the APhw prolongation by $\alpha\beta$-meATP outlasted the membrane depolarization, in that the APhw returned to control values 2.53 ± 0.51 s ($n = 10$) after the onset of application, which lasted only for 100 ms. Hence, these data are consistent with a P2XR-mediated activation of the Ca^{2+}-dependent second messenger signalling cascade in BCs (Milenkovic *et al.* 2009).

In vivo experiments in Figs 1 and 4 demonstrated that P2X2/3R-activation shortens the EPSP-AP time, thereby shifting the timing of the AP peak and, thus contributing to temporal properties of APs. To validate this finding under the constant firing at physiological rate (50 Hz), the latency of synaptically-evoked APs was measured before, during and after the $\alpha\beta$-meATP application (Fig. 5*D*, left). The AP latency (time between the stimulus artefact and the AP peak) gradually decreased by up to 10% 200 ms after the puff onset. This effect clearly outlasted the agonist application (puff duration 100 ms) and the AP latency returned to control values 1.06 s after the puff-onset (mean ± SEM AP latency for time periods relative to puff onset: 0.2–1 s = 0.84 ± 0.009 ms, 1–1.8 s = 0.77 ± 0.008 ms and 1.8–2.6 s = 0.84 ± 0.009 ms, $n = 10$, $P < 0.001$, RM ANOVA). The maximum shortening of the latency was 100 ± 40 μs at 200–400 ms after the puff onset (for each cell, measurements were based on averages of 10 successive APs; mean ± SEM, $n = 9$). Shorter latencies were seen up to 800 ms after the $\alpha\beta$-meATP application, indicating a long lasting effect (mean ± SEM AP latency difference from control for 0.2–1 s = −13 ± 2 μs, $P = 0.79$; 1.2–2 s = –84 ± 30 μs, $P = 0.04$; 2–2.6 s = 15 ± 4 μs, $P = 0.09$; $n = 9$, one sample *t* test) (Fig. 5*D*, right). Taken together, these data confirm the impact of P2X2/3R on the precision of APs firing and additionally provide evidence that this modulation can persist for seconds.

P2XR and glutamate receptors (GluR) were shown in close proximity at synapses in hippocampus and cerebellum and their functional interaction was described in hippocampal pyramidal neurons (Rubio and Soto, 2001; Pankratov *et al.* 2002; Volonte *et al.* 2006). To investigate whether the activation of P2X2/3R may directly affect the transmission via GluR, we assessed the effect of $\alpha\beta$-meATP puff application on pharmacologically isolated glutamatergic postsynaptic currents (EPSCs). The experiments were conducted using the same protocol as in Fig. 5, only in voltage clamp. Data analysis showed neither an effect of $\alpha\beta$-meATP on the EPCS amplitudes, nor on the decay time constants throughout the train (I_{EPSC} $\alpha\beta$-meATP *vs.* control: effect of time $P = 0.9$, effect of treatment $P = 0.2$, interaction time × treatment $P = 0.9$; τ_{wd} $\alpha\beta$-meATP *vs.* control: effect of time $P = 0.1$, effect of treatment $P = 0.6$, interaction time × treatment $P = 0.7$, $n = 10$, two-way RM ANOVA, data not shown). Thus, we conclude that the modulatory effect on AP properties through P2X2/3R does not engage the GluR and occurs downstream of glutamatergic transmission.

Purinergic modulation is cell-specific and tonotopically-determined

Our data show a differentiation of BCs with regard to responsiveness to ATP (responders *vs.* non-responders). To examine whether the observed differences reflect developmental changes of purinergic effects related to the topographic/tonotopic nuclear organization, the responsiveness of neurons was assessed considering their

localization within the nucleus. Pre-hearing neurons were investigated with whole-cell recordings in parasagittal slices and puff application of $\alpha\beta$-meATP. After hearing onset, *in vivo* recordings were performed with acoustic stimulation and iontophoretic application of a P2X2/3R antagonist. To enable the best possible comparison of slice and *in vivo* data, the period just after hearing onset was investigated with both approaches (slice: P13–16, *in vivo*: P13–15). With slice recordings, a total of 128 cells were recorded and sorted into four age groups: P4, P6–7, P10–12 and P13–16. Neurons were labelled with biocytin, which enabled morphological characterization and *post-hoc* reconstruction of their topographic position (Fig. 6*A*). Neurons from P4 animals could not be reliably identified as BCs or stellate cells as a result of their immature morphology and electrophysiological properties. Still, they were classified as responders and non-responders based on the reaction to puff application of $\alpha\beta$-meATP (Fig. 6*A*, P4). From P6 onward, all cells that showed responses to agonist application were unambiguously identified as BCs. Between P6 and P16, the nuclear area of responders progressively narrowed and became restricted to the area just rostral of the AN root (Fig. 6*A*, P6–7, P10–12, P13–16). Quantification of the data in the rostral AVCN showed that the vast majority of cells responded to $\alpha\beta$-meATP before hearing onset (P4 = 72%, P6–7 = 91%, P10–12 = 93%), whereas the percentage of responders largely reduced thereafter (P13–16 = 33%). In the area dorsal to the AN (Fig. 6*A*), the percentage of responders gradually decreased with maturation and dropped significantly in the P10–12 group (P4 = 83%, P10–12 = 11%, $P = 0.03$, χ^2 test). Finally, out of 28 cells recorded between P4 and P16 in the caudal VCN, only one responded to $\alpha\beta$-meATP.

In vivo recordings with acoustic stimulation in animals after hearing onset allowed to capture the effects of P2X2/3R-antagonist along with the characteristic frequency of respective units. In the AVCN, characteristic frequencies of neurons show an orderly representation, with low frequencies located rostroventrally and higher frequencies arranged towards dorso-caudal positions (Muller, 1996). The nuclear tonotopy was reconstructed from multi-unit recordings in parasagittal nuclear planes based on rostro-caudal, dorsoventral and mediolateral stereotaxic co-ordinates with reference to fluorogold bulk-labelling conducted at the end of the recording session. The topographic position of each recorded unit was then determined according to its stereotaxic co-ordinates (Fig. 6*B–D*). Bushy cells were physiologically identified by their primary-like peristimulus time histogram and the complex waveform including the discernible prepotentials (Englitz *et al.* 2009). A total of 87 BCs were recorded from four developmental stages: P13–15, P16–17, P20–23 and >P60. Iontophoretic glycine application was used as a positive control for the function of multibarrel electrode. Although glycine completely blocked APs in all BCs, just 40–45% of low-frequency BCs from P13–15, P16–17 and P20–23 showed a modulation by P2X2/3R. The respective effect was discerned by a significant decrease of spontaneous firing upon antagonizing the P2X2/3R with AF-353 or TNP-ATP ($z > 1.65$) (Fig. 6*D* and *E*). None of the units with CF>5 kHz in P16–17 animals and CF>10 kHz in P20–23 animals responded to antagonist application. In P13–15 animals, no units with CF > 6 kHz were recorded because of the delayed maturation of the high-frequency cochlear domain (Rübsamen, 1992). Both in P16–17 and P20–23 gerbils, purinergic modulation contributed to AP firing only in low-CF units ($n = 17$, $P = 0.011$, $r_s = 0.6$ and $n = 33$, $P = 0.04$, $r_s = 0.36$, respectively, Spearman's rank order correlation). None of the eleven BCs in >P60 animals responded to TNP-ATP or AF-353 application (data not shown), which is consistent with a proposed role of purinergic signalling in postnatal development (Dietz *et al.* 2012). Taken together, the slice and *in vivo* data suggest that purinergic modulation engages BCs throughout the rostral- and the dorsal-area of the AVCN before hearing onset. Up to the fourth postnatal week, the area of ATP-responsive BCs becomes constrained to the low-frequency units in the rostral AVCN.

In slice and *in vivo* experiments in the CN, it has been shown that stellate cells which are intermingled with BCs do not respond to P2XR agonists (Milenkovic *et al.* 2009; Dietz *et al.* 2012). These findings were reviewed in the present study by testing whether stellate cells may be modulated by ATP at different developmental stages then BCs and/or whether such modulation may be linked to a defined range of CFs. Physiologically, stellate cells can be identified by their biphasic waveform and chopper peristimulus time histogram (Young *et al.* 1988; Typlt *et al.* 2012). Recordings from 15 stellate cells across four developmental stages (from P13 to $P > 60$) with CFs between 0.15 and 27.5 kHz showed no response to TNP-ATP or AF-353 ($z < 1.65$) (Fig. 6*D* and *E*).

The developmental down-regulation of purinergic responses in BCs follows a similar time course as the respective decrease in input resistance (Dietz *et al.* 2012). Therefore, it was necessary to rule out the possibility that BCs in different regions have different input resistance(R_{in}), which might account for the lack of response to $\alpha\beta$-meATP in some of the neurons. The respective analysis showed a general reduction in R_{in} but no difference with respect to the neurons' topographic location (R_{in} in BCs effect of maturity $P < 0.001$; effect of position $P = 0.49$; P4, $n = 20$; P6–7, $n = 19$; P10–12, $n = 26$; P13–16, $n = 24$; two-way ANOVA, data not shown). Hence, it can be concluded that purinergic modulation is specific for the topographic position of BCs in the CN, which also determines the developmental time course of responses.

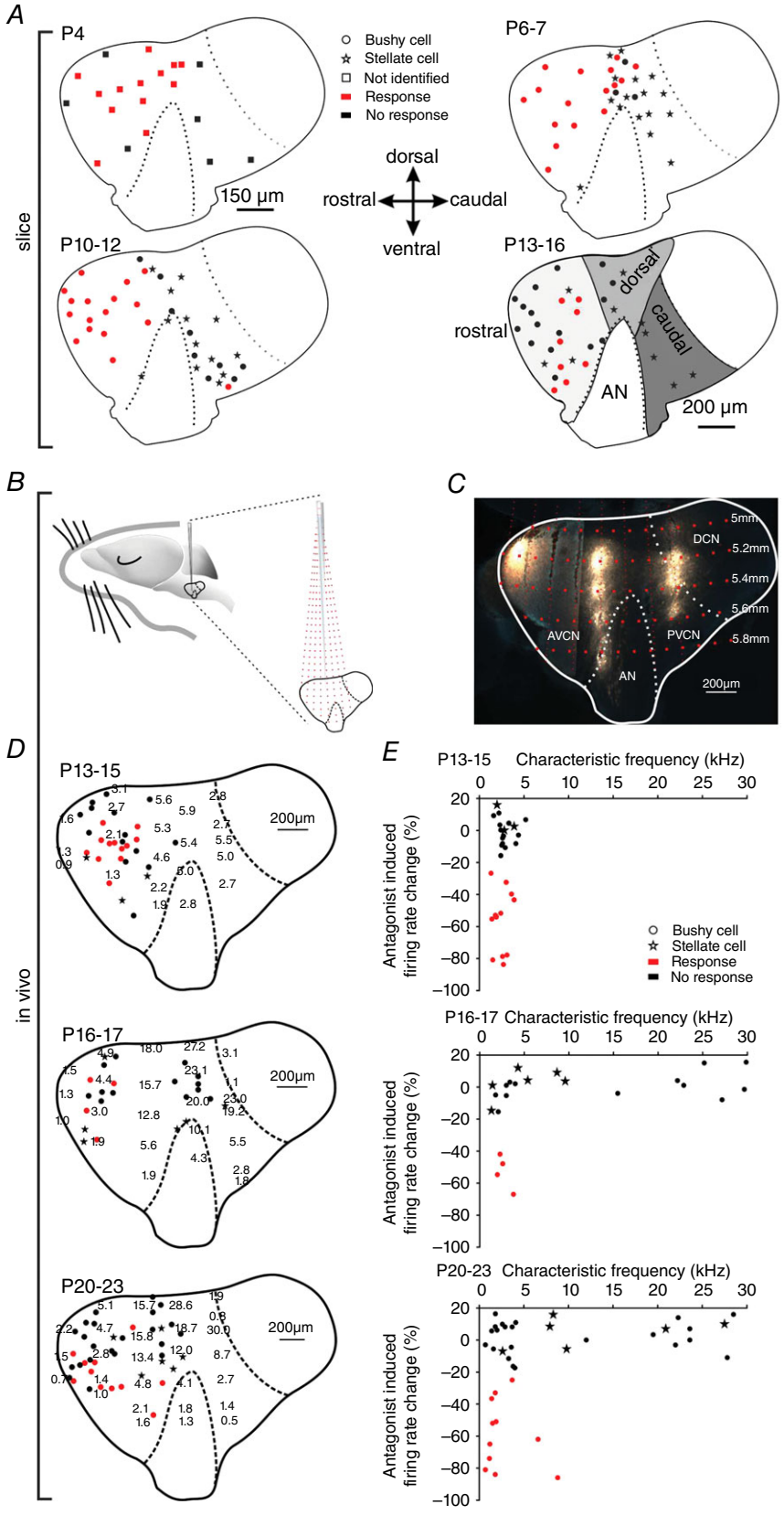

Figure 6. Purinergic modulation is cell-specific and dependent on characteristic frequency
A, parasagittal view to the CN of P4 (upper left), P6–7 (upper right), P10–12 (lower left), P13–16 (lower right) animals showing the positions of recorded cells. Red symbols indicate cell affected by puff application of $\alpha\beta$-meATP (responders; $^{***}P < 0.001$, z test), black symbols non-responders; stars show stellate cells. At P4, recorded cells are indicated by squares since they could not be unambiguously characterized as bushy or stellate. Grey areas on the P13–16 slice schematically depict the rostral, dorsal and caudal region. Cells from all ages were sorted accordingly. *B*, schematic drawing of the experimental approach used for tonotopic mapping in the cochlear nucleus complex. Red dashed lines show electrode trajectories targeting at different positions within the CN, red dots indicate the depth of the electrode penetration. *C*, parasagittal slice of the gerbil CN labelled*in vivo* with fluorogold at three rostro-caudal penetration positions in 200 μm vertical steps. The image was generated by overlaying two medio-laterally separated slices; the curvature of the CN along the rostro-caudal axis precludes a visualization of the entire information in one slice. *D*, distribution of CFs (kHz) in P13–15 (upper panel), P16–17 (middle panel) and P20–23 cells (lower panel). Positions of BCs are indicated by closed circles, stellate cells by stars. Red dots show BCs with significant reduction of spontaneous firing during application of AF-353 or TNP-ATP (responders, $z > 1.65$); black dots show BCs not susceptible to antagonists (non-responders). *E*, relative changes in firing rates upon application of P2X2/3R antagonist as a function of the CF of the unit. The effect on BCs depended on the CF of the unit (P16–17: $P = 0.011$, $r_s = 0.6$; P20–23: $P = 0.04$, $r_s = 0.36$; Spearman's rank order correlation). Note that none of the stellate cells were susceptible to P2X2/3R antagonists. [Colour figure can be viewed at wileyonlinelibrary.com]

Developmental shift from P2X2/3R to AMPA receptor (AMPAR) responses

During the postnatal development, excitatory transmission at calyceal synapses becomes increasingly fast and potent via a change in GluR composition and increase in AMPAR quantal component (Isaacson and Walmsley, 1996; Taschenberger and von Gersdorff, 2000; Futai *et al.* 2001; Joshi *et al.* 2004; Lu and Trussell, 2007). Considering modulatory effect of ATP on the AP shape, the properties of APs elicited through AMPAR or P2X2/3R activation were compared (Fig. 7*A*). Puff application was set to evoke suprathreshold responses to both agonists in P6–7 BCs from the rostral AVCN (AMPA 50 μM, $\alpha\beta$-meATP 100 μM, both 100 ms). The APs elicited by $\alpha\beta$-meATP had on average 40% longer APhw at RT (APhw AMPA = 1.59 ± 0.12 ms, n = 10; $\alpha\beta$-meATP = 2.24 ± 0.23 ms, n = 9; P = 0.04, t test). These results provide additional evidence that the P2X2/3R prolong the APs of immature neurons, prior to the more rapid AMPA-mediated signalling which is required for auditory signal processing.

To track down the developmental time course of P2X2/3R- and AMPAR-mediated currents, we performed whole-cell voltage clamp recordings (V_{hold} = −60 mV) and compared $I_{P2X2/3}$ and I_{AMPA} evoked by puff applications to the same cells, considering the topographic position and the postnatal age (Fig. 7*B*). The rationale was to compare saturating current responses, rather than comparing the puff-evoked $I_{P2X2/3}$ with synaptically-evoked AMPA EPSCs. In P6–7, BCs from the rostral and dorsal region were more potently activated through P2X2/3R than through AMPAR ($I_{P2X2/3}/I_{AMPA}$ rostral = 1.9 ± 0.3, n = 10, AN = 1.2 ± 0.6, n = 9). With increasing maturity, $I_{P2X2/3}$ remained larger than I_{AMPA} only in the rostral AVCN, whereas the respective current ratio changed in favour of AMPAR in the dorsal region (P10–12 $I_{P2X2/3}/I_{AMPA}$ rostral = 1.9 ± 0.4, n = 15, dorsal = 0.1 ± 0.1, n = 4). Comparison of the population data for P10–12 and P13–16 BCs from the rostral pole revealed a 2.3-fold increase in I_{AMPA} and a one-third decrease in $I_{P2X2/3}$. This explains a significantly smaller current ratio at P13–16 with respect to both prehearing groups ($I_{P2X2/3}/I_{AMPA}$ effect of maturity $P < 0.001$; effect of position P = 0.001, two-way ANOVA) (Fig. 7*B*). I_{AMPA} showed a general developmental increase in all regions (effect of maturity $P < 0.001$ two-way ANOVA). Taken together, these results indicate that the developmental shift from P2X2/3R to AMPAR mediated signalling follows a topographically predetermined time course.

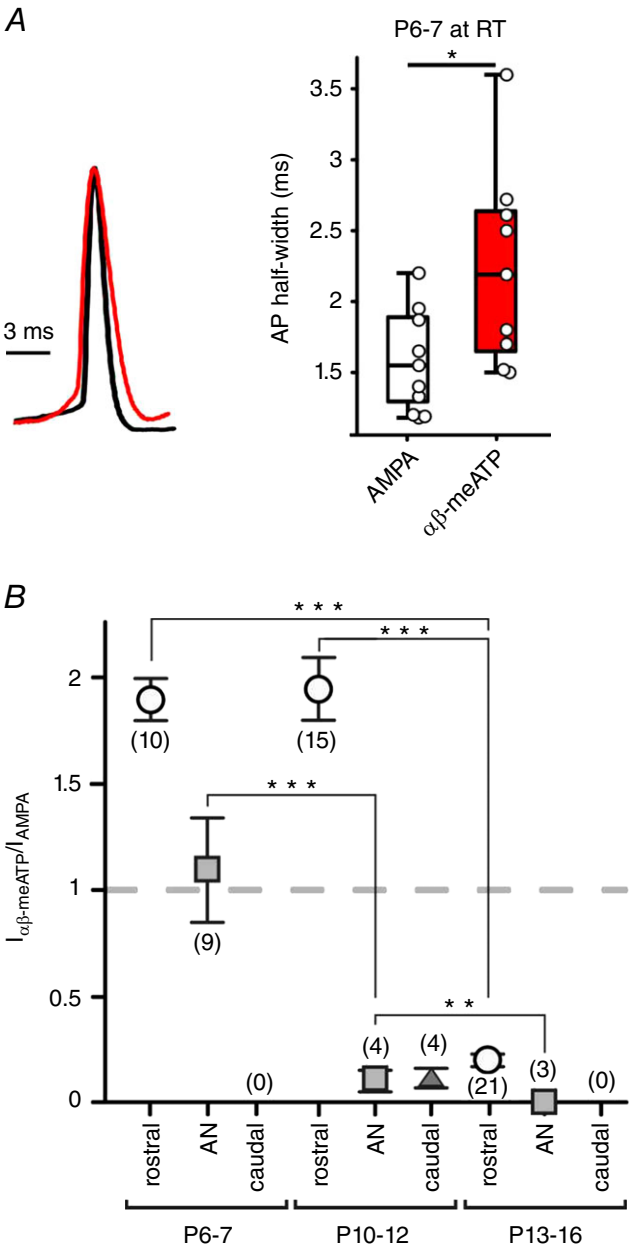

Figure 7. Developmental shift from P2X2/3R- to AMPAR-mediated signalling in the VCN
A, comparison of the APs evoked either by $\alpha\beta$-meATP- or by AMPA-puff application to P6–7 BCs from the rostral VCN (100 and 50 μM, respectively; both 100 ms). Overlay of peak-normalized APs (left) and summary data (right) (*$P < 0.05$, t test). *B*, responsiveness of BCs with respect to topographic VCN position (rostral-dots, auditory nerve root region AN, squares; caudal, triangle) and age. Whole-cell currents evoked in the same cells by separate puff applications of $\alpha\beta$-meATP and AMPA in saturating concentrations show specific developmental patterns. Note a prominent reduction in $I_{\alpha\beta\text{-meATP}}/I_{AMPA}$ ratio occurring before hearing onset in the auditory nerve region (squares) and after hearing onset in the rostral region (dots). In the caudal region, $\alpha\beta$-meATP response was either very weak (triangle) or completely missing. Numbers of cells are given in parentheses. No responder BCs were found in the caudal VCN indicated by (0) (**$P < 0.01$, ***$P < 0.001$ two-way ANOVA). [Colour figure can be viewed at wileyonlinelibrary.com]

Discussion

The present study provides evidence that BCs integrate glutamatergic input from the endbulb of Held with

paracrine ATP signalling to facilitate AP generation and prolong APs during early postnatal development. Combination of slice recordings before hearing onset and *in vivo* recordings with iontophoretic drug applications after hearing onset revealed an orderly tonotopic sequence of purinergic effects during postnatal development of the VCN. In high-frequency regions, P2X2/3R-mediated modulation of BCs disappears before hearing onset. In low-to-mid frequency regions, the respective modulation is reduced around hearing onset, leaving only a subset of low frequency BC (CF $<$ 10 kHz) susceptible to endogenous ATP up to P20–23. This tonotopic down-regulation of P2X2/3R currents goes hand in hand with an increase in AMPAR currents. After hearing onset, BCs in high-frequency regions only utilize AMPA signalling, whereas BCs in the low-to-mid-frequency area still show weak P2X2/3R effects that augment AMPAR-currents. BCs engaged with ATP modulation have shorter EPSP-AP delay and longer APs. Previously, it was shown that P2XR activation triggers a Ca^{2+}-dependent mechanism that activates PKC and thereby facilitates firing in maturing BCs (Milenkovic *et al.* 2009). Such long-lasting changes in intrinsic excitability persisting for seconds are probably mediated by second messengers (Zhang and Linden, 2003). Taken together, these results suggest that ATP signalling tightly regulates the excitability of BCs and AP duration during early postnatal development. Such topographically-specific modulation occurs during the period of structural refinement that leads to tonotopic map sharpening and the ensuing strengthening of the endbulb of Held inputs.

Detailed pharmacological characterization enabled identification of the heteromeric P2X2/3R as the mediator of ATP effects. Based on these findings, it was possible to closely examine the ATP modulation *in vivo* by targeting P2X2/3R with specific antagonists. These findings will also justify conclusions to be drawn from future studies in $P2X2^{-/-}$:$P2X3^{-/-}$ mice (Cockayne *et al.* 2005). As a result of prominent Ca^{2+} permeability, low desensitization and high sensitivity to ATP (Coddou *et al.* 2011; Li *et al.* 2013), the P2X2/3R is ideally suited to contribute to Ca^{2+}-dependent maturational processes, triggered by ATP release from an as yet unknown source (Dietz *et al.* 2012).

Fine-tuning of neuronal activity during postnatal development

Maturation of the central auditory system starts with an initial circuit formation, followed by structural and functional refinement, which generates the precise tonotopic organization crucial for the differential processing of complex sounds in adults (Sanes and Siverls 1991; Rubel and Fritzsch 2002; Kandler, 2004). Refinement of the genetically laid-out circuits, guided by precise patterns of spontaneous activity before hearing onset, affects both the excitatory and inhibitory afferent synapses (Sanes and Constantine-Paton, 1983, 1985; Aponte *et al.* 1996; Kotak and Sanes 2000; Kim and Kandler 2003; Leao *et al.* 2004; Walmsley *et al.* 2006; Erazo-Fischer *et al.* 2007; McKay and Oleskevich, 2007; Hirtz *et al.* 2011; Clause *et al.* 2014; Wright *et al.* 2014). During this critical period, the activity of endbulb of Held-BC synapse can be enhanced by ATP (Dietz *et al.* 2012), whereas serotonin amplifies the activity of inhibitory synapses in the lateral superior olive (Fitzgerald and Sanes, 1999). Finally, the fine-tuning plasticity changes controlled by the acoustically evoked activity become effective during early processing of acoustic information (Sanes and Takacs, 1993; Kapfer *et al.* 2002; Knudsen 2002; Seidl and Grothe, 2005; Leake *et al.* 2006; Werthat *et al.* 2008; Sanes and Bao, 2009). The information relevant for these maturational processes is inherent in the activity patterns and in the time scale of AP discharges (Butts *et al.* 2007; Shah and Crair, 2008; Blankenship and Feller, 2010; Kirkby *et al.* 2013).

Before hearing onset, discrete bursts of APs are generated in the immature cochlea and, from there, are conveyed along the afferent central auditory pathways (Rübsamen and Schäfer, 1990; Lippe, 1994; Jones *et al.* 2007; Sonntag *et al.* 2009; Tritsch *et al.* 2010). The fine temporal structure of the still immature IHC activity is regulated by multiple signalling mechanisms: (i) spontaneous Ca^{2+}-elicited APs that show position-dependent patterns along the cochlea (Kros *et al.* 1998; Tritsch *et al.* 2010; Johnson *et al.* 2011; Johnson *et al.* 2012); (ii) activity synchronization of neighbouring IHC through endogenous ATP (Tritsch *et al.* 2007; Tritsch and Bergles, 2010); and (iii) modulation of spiking pattern by release of ACh from efferent olivo-cochlear fibres (Glowatzki and Fuchs, 2000; Johnson *et al.* 2011; Johnson *et al.* 2013*b*). Taken together, these mechanisms generate a topographically specific firing pattern necessary for maturation of the synaptic machinery of IHC ribbon synapses before hearing onset (Johnson *et al.* 2011; Johnson *et al.* 2013*a*). The present study shows that, also in the brainstem, a specific regulatory mechanism attunes the APs in a cell- and tonotopically-dependent manner. Accordingly, we propose that, early after birth, ATP contributes to the activity of BCs located rostrally and dorsally to the AN root region, although not to those in a caudal position within the VCN. In most parts of the VCN, ATP signalling diminished with the onset of acoustically evoked signal processing. Thereafter, only BCs in low-frequency region integrate the P2X2/3R signalling with glutamatergic input from the AN terminal. Interaction of the two signalling pathways occurs downstream of GluR, as indicated by the lack of an effect of P2X2/3R on the EPSCs. Facilitated AP generation, measured as increased firing frequency, shorter EPSP-AP delay *in vivo* and a shorter AP latency in slice experiments

is consistent with a P2X2/3R-mediated increase in synaptic efficacy. The underlying mechanism probably includes P2XR-mediated Ca^{2+} signals that were shown to last for several seconds in the BC soma (Milenkovic *et al.* 2009; Dietz *et al.* 2012). It is conceivable that such mechanism could trigger Ca^{2+}-dependent potentiation as shown in hippocampal pyramidal neurons (Malenka, 1991; Fricker and Miles, 2000; Campanac and Debanne, 2008). This assumption is supported by our earlier finding indicating that extracellular ATP potentiates otherwise subthreshold depolarization to evoke APs (Milenkovic *et al.* 2009). The presumably important role of Ca^{2+} is also demonstrated in the present study by showing that prolongation of synaptically evoked APs could not be evoked by membrane depolarization *per se* but required P2X2/3R activation. Thus, P2X2/3R signalling might compensate for the still incomplete strength of synaptic transmission and the prevailing AMPAR desensitization, which are both characteristics of the immature endbulb of Held synapse (Bellingham *et al.* 1998; Brenowitz and Trussell, 2001; Chanda and Xu-Friedman, 2010).

During spontaneous activity in mature gerbils, synaptic transmission at the endbulb-BC synapse shows an AP failure rate of ∼25% as a result of subthreshold EPSPs (Keine and Rübsamen, 2015). In the present study, we show that AP facilitation through endogenous ATP increases the fidelity of AP transmission at the immature endbulb of Held-BC synapse. This can be presumed from the 24% increase in firing rates following $\alpha\beta$-meATP application *in vivo* (Fig. 4*B*). The fact that, under these conditions, all APs recorded from BCs are preceded by prepotentials (i.e. presynaptic APs) strengthens the assumption of a P2X2/3R-mediated increase in the reliability of immature endbulb of Held synapse. Quantification of isolated EPSPs (AP transmission failures) before and after application of P2X2/3R antagonists would be an approach to test this hypothesis further. However, this is probably not possible from *in vivo* recordings with multibarrel electrodes. Nevertheless, the P2X2/3R activation appears to shorten the integration time for AP generation, rather than directly elicit postsynaptic APs in BCs. Earlier, we have shown *in vivo* that, after blockade of glutamatergic transmission and the ensuing loss of APs, iontophoretic application of ATP can partially restore firing (Dietz *et al.* 2012). Hence, it was concluded that extracellularly applied ATP can evoke APs *per se*. In the present study, we used P2X2/3R antagonists to obtain a better understanding of the physiological effects of endogenously released ATP. Under these conditions, no isolated postsynaptic APs were observed, suggesting that the concentration of ATP *in vivo* is sufficient to boost the glutamatergic input but not to elicit additional APs. Such increased synaptic efficacy probably provides associative signals at fast time scales required for Hebbian synaptic strengthening (Markram *et al.* 1997; Buonomano and Merzenich, 1998; Abbott and Nelson, 2000; Song *et al.* 2000; Caporale and Dan, 2008). Similar mechanisms were shown to contribute to the development of retinotopic maps, where Hebbian plasticity governs the spike time-dependent maturation of synapses extending to the period of early visual experience (Katz and Shatz, 1996; Buonomano and Merzenich, 1998; Karmarkar and Dan, 2006; Butts and Kanold, 2010).

Tonotopic pattern of functional maturation

The APs in responder BCs have 22% longer APhw *in vivo* than non-responder BCs. Brief APs, low excitability and high temporal precision of discharges are predominantly maintained through Kv3 and Kv1 conductances (Manis and Marx, 1991; Cao *et al.* 2007) and considered as markers of mature BCs. In immature BCs, the Ca^{2+}-PKC signalling cascade activated by extracellular ATP probably attenuates both of these conductances (Milenkovic *et al.* 2009), which is in agreement with longer APs and increased excitability presently observed in responder cells. Modulation of the Kv conductance may endow immature BCs with prolonged APs, which is assumed to enable larger Ca^{2+} entry through high-voltage activated channels (McCobb and Beam, 1991). Bushy cells from P6–14 rats were shown to express somatic L, N and R-type channels (Doughty *et al.* 1998). In addition to the pathway through voltage-dependent Ca^{2+}-channels, the activation of P2X2/3R provides a direct pathway for substantial Ca^{2+} entry that is less dependent on membrane depolarization (Egan and Khakh, 2004; Pankratov *et al.* 2009). Taken together, previously published data showing prominent somatic Ca^{2+} signals upon P2XR activation (Milenkovic *et al.* 2009; Dietz *et al.* 2012) and the presently shown effect on synaptic efficacy imply that such signalling could guide the plasticity changes involved in the functional maturation of synaptic contacts (Zucker, 1999; Flavell and Greenberg, 2008; Pankratov *et al.* 2009; Rosenberg and Spitzer, 2011). Notably, the developmental loss of P2X2/3R responses was accompanied with an increase in AMPAR currents. Taking this into account, it is plausible to hypothesize that low-frequency BCs retaining ATP responsiveness up to the forth postnatal week have delayed development compared to BCs from high-frequency regions. Such a developmental pattern indicates that early auditory experience could be required for maturation of endbulb of Held-BC synapses in the low frequency region. Because the cochleotopic sharpening of AN terminals apparently occurs prior to early auditory experience (Leake *et al.* 2006), it is conceivable that sound-evoked activity contributes to synaptic strengthening rather than to structural refinement. The developmental pattern along the high-to-low frequency axis is consistent with the sequential development of calyx of Held synapses in the MNTB of gerbils, which extends beyond hearing onset

only in the low-frequency region (Ford *et al.* 2009). The MNTB PNs were also shown to be modulated by ATP before hearing onset, although, at P8, the membrane current and depolarization were smaller than in BCs of the same age (Dietz *et al.* 2012). It remains to be clarified whether the purinergic modulation in the MNTB follows a similar tonotopic pattern during development, which may indicate a general role of ATP in development of calyceal synapses. Nevertheless, the morphological maturation of the calyx terminal and biophysical maturation of the PN progress in parallel and developmental information is apparently provided in the synchronous pre-to-post activity (Hoffpauir *et al.* 2010). The present study suggests that the paracrine ATP signalling probably contributes to the maturation of the endbulb of Held-BC synapse by increasing the postsynaptic response to the presynaptic input.

References

Abbott LF & Nelson SB (2000). Synaptic plasticity: taming the beast. *Nat Neurosci* **3**, 1178–1183.

Anderson-Sprecher R (1994). Model comparisons and R^2. *AmStat* **48**, 113–117.

Aponte JE, Kotak VC & Sanes DH (1996). Decreased synaptic inhibition leads to dendritic hypertrophy prior to the onset of hearing. *AudNeurosci* **2**, 235–240.

Baqi Y, Hausmann R, Rosefort C, Rettinger J, Schmalzing G & Müller CE (2011). Discovery of potent competitive antagonists and positive modulators of the P2X2 receptor. *J Med Chem* **54**, 817–830.

Bean BP (2007). The action potential in mammalian central neurons. *Nat Rev Neurosci* **8**, 451–465.

Bellingham MC, Lim R & Walmsley B (1998). Developmental changes in EPSC quantal size and quantal content at a central glutamatergic synapse in rat. *J Physiol* **511**, 861–869.

Blackburn CC & Sachs MB (1989). Classification of unit types in the anteroventral cochlear nucleus. PST histograms and regularity analysis. *J Neurophysiol* **62**, 1303–1329.

Blankenship AG & Feller MB (2010). Mechanisms underlying spontaneous patterned activity in developing neural circuits. *Nat Rev Neurosci* **11**, 18–29.

Brenowitz S & Trussell LO (2001). Minimizing synaptic depression by control of release probability. *J Neurosci* **21**, 1857–67.

Buonomano DV & Merzenich MM (1998). Cortical plasticity: from synapses to maps. *Annu Rev Neurosci* **21**, 149–186.

Butts DA & Kanold PO (2010). The applicability of spike time dependent plasticity to development. *Front Synaptic Neurosci* **2**, 30.

Butts DA, Kanold PO & Shatz CJ (2007). A burst-based 'Hebbian' learning rule at retinogeniculate synapses links retinal waves to activity-dependent refinement. *PLoS Biol* **5**, e61.

Campanac E & Debanne D (2008). Spike timing-dependent plasticity: a learning rule for dendritic integration in rat CA1 pyramidal neurons. *J Physiol* **586**, 779–793.

Cang J & Feldheim DA (2013). Developmental mechanisms of topographic map formation and alignment. *Annu Rev Neurosci* **36**, 51–77.

Cao XJ, Shatadal S & Oertel D (2007). Voltage-sensitive conductances of bushy cells of the Mammalian ventral cochlear nucleus. *J Neurophysiol* **97**, 3961–3975.

Caporale N & Dan Y (2008). Spike timing-dependent plasticity: a Hebbian learning rule. *Annu Rev Neurosci* **31**, 25–46.

Chanda S & Xu-Friedman MA (2010). A low-affinity antagonist reveals saturation and desensitization in mature synapses in the auditory brain stem. *J Neurophysiol* **103**, 1915–1926.

Clause A, Kim G, Sonntag M, Weisz CJ, Vetter DE, Rubsamen R & Kandler K (2014). The precise temporal pattern of prehearing spontaneous activity is necessary for tonotopic map refinement. *Neuron* **82**, 822–835.

Cockayne DA, Dunn PM, Zhong Y, Rong W, Hamilton SG, Knight GE, Ruan HZ, Ma B, Yip P, Nunn P, McMahon SB, Burnstock G & Ford AP (2005). P2X2 knockout mice and P2X2/P2X3 double knockout mice reveal a role for the P2X2 receptor subunit in mediating multiple sensory effects of ATP. *J Physiol* **567**, 621–639.

Coddou C, Yan Z, Obsil T, Huidobro-Toro JP & Stojilkovic SS (2011). Activation and regulation of purinergic P2X receptor channels. *Pharmacol Rev* **63**, 641–683.

Davis RL (2003). Gradients of neurotrophins, ion channels, and tuning in the cochlea. *Neuroscientist* **9**, 311–316.

Dehmel S, Kopp-Scheinpflug C, Weick M, Dorrscheidt GJ & Rubsamen R (2010). Transmission of phase-coupling accuracy from the auditory nerve to spherical bushy cells in the Mongolian gerbil. *Hear Res* **268**, 234–249.

Dietz B, Jovanovic S, Wielsch B, Nerlich J, Rubsamen R & Milenkovic I (2012). Purinergic modulation of neuronal activity in developing auditory brainstem. *J Neurosci* **32**, 10699–10712.

Doughty JM, Barnes-Davies M, Rusznak Z, Harasztosi C & Forsythe ID (1998). Contrasting Ca^{2+} channel subtypes at cell bodies and synaptic terminals of rat anterioventral cochlear bushy neurones. *J Physiol* **512**, 365–376.

Egan TM & Khakh BS (2004). Contribution of calcium ions to P2X channel responses. *J Neurosci* **24**, 3413–3420.

Englitz B, Tolnai S, Typlt M, Jost J & Rubsamen R (2009). Reliability of synaptic transmission at the synapses of Held in vivo under acoustic stimulation. *PloS ONE* **4**, e7014.

Erazo-Fischer E, Striessnig J & Taschenberger H (2007). The role of physiological afferent nerve activity during in vivo maturation of the calyx of Held synapse. *J Neurosci* **27**, 1725–1737.

Fitzgerald KK & Sanes DH (1999). Serotonergic modulation of synapses in the developing gerbil lateral superior olive. *J Neurophysiol* **81**, 2743–2752.

Flavell SW & Greenberg ME (2008). Signaling mechanisms linking neuronal activity to gene expression and plasticity of the nervous system. *Annu Rev Neurosci* **31**, 563–590.

Ford MC, Grothe B & Klug A (2009). Fenestration of the calyx of Held occurs sequentially along the tonotopic axis, is influenced by afferent activity, and facilitates glutamate clearance. *JComp Neurol* **514**, 92–106.

Francis HW & Manis PB (2000). Effects of deafferentation on the electrophysiology of ventral cochlear nucleus neurons. *Hear Res* **149**, 91–105.

Friauf E & Lohmann C (1999). Development of auditory brainstem circuitry. Activity-dependent and activity-independent processes. *Cell Tissue Res* **297**, 187–195.

Fricker D & Miles R (2000). EPSP amplification and the precision of spike timing in hippocampal neurons. *Neuron* **28**, 559–569.

Futai K, Okada M, Matsuyama K & Takahashi T (2001). High-fidelity transmission acquired via a developmental decrease in NMDA receptor expression at an auditory synapse. *J Neurosci* **21**, 3342–3349.

Gever JR, Cockayne DA, Dillon MP, Burnstock G & Ford AP (2006). Pharmacology of P2X channels. *Pflügers Arch* **452**, 513–537.

Glowatzki E & Fuchs PA (2000). Cholinergic synaptic inhibition of inner hair cells in the neonatal mammalian cochlea. *Science* **288**, 2366–2368.

Hackney CM, Osen KK & Kolston J (1990). Anatomy of the cochlear nuclear complex of guinea pig. *Anat Embryol* **182**, 123–149.

Hanganu-Opatz IL (2010). Between molecules and experience. role of early patterns of coordinated activity for the development of cortical maps and sensory abilities. *Brain Res Rev* **64**, 160–176.

Havey DC & Caspary DM (1980). A simple technique for constructing 'piggy-back' multibarrel microelectrodes. *Electroencephalogr Clin Neurophysiol* **48**, 249–251.

Hirtz JJ, Boesen M, Braun N, Deitmer JW, Kramer F, Lohr C, Muller B, Nothwang HG, Striessnig J, Lohrke S & Friauf E (2011). Cav1.3 calcium channels are required for normal development of the auditory brainstem. *J Neurosci* **31**, 8280–8294.

Hoffpauir BK, Kolson DR, Mathers PH & Spirou GA (2010). Maturation of synaptic partners: functional phenotype and synaptic organization tuned in synchrony. *J Physiol* **588**, 4365–4385.

Inan M & Crair MC (2007). Development of cortical maps. perspectives from the barrel cortex. *Neuroscientist* **13**, 49–61.

Isaacson JS & Walmsley B (1996). Amplitude and time course of spontaneous and evoked excitatory postsynaptic currents in bushy cells of the anteroventral cochlear nucleus. *J Neurophysiol* **76**, 1566–1571.

Jarvis MF & Khakh BS (2009). ATP-gated P2X cation-channels. *Neuropharmacology* **56**, 208–215.

Johnson SL, Eckrich T, Kuhn S, Zampini V, Franz C, Ranatunga KM, Roberts TP, Masetto S, Knipper M, Kros CJ & Marcotti W (2011). Position-dependent patterning of spontaneous action potentials in immature cochlear inner hair cells. *Nat Neurosci* **14**, 711–717.

Johnson SL, Kennedy HJ, Holley MC, Fettiplace R & Marcotti W (2012). The resting transducer current drives spontaneous activity in prehearing mammalian cochlear inner hair cells. *J Neurosci* **32**, 10479–10483.

Johnson SL, Kuhn S, Franz C, Ingham N, Furness DN, Knipper M, Steel KP, Adelman JP, Holley MC & Marcotti W (2013*a*). Presynaptic maturation in auditory hair cells requires a critical period of sensory-independent spiking activity. *PNAS* **110**, 8720–8725.

Johnson SL, Wedemeyer C, Vetter DE, Adachi R, Holley MC, Elgoyhen AB & Marcotti W (2013*b*). Cholinergic efferent synaptic transmission regulates the maturation of auditory hair cell ribbon synapses. *Open Biol* **3**, 130163.

Jones TA, Leake PA, Snyder RL, Stakhovskaya O & Bonham B (2007). Spontaneous discharge patterns in cochlear spiral ganglion cells before the onset of hearing in cats. *J Neurophysiol* **98**, 1898–1908.

Joshi I, Shokralla S, Titis P & Wang LY (2004). The role of AMPA receptor gating in the development of high-fidelity neurotransmission at the calyx of Held synapse. *J Neurosci* **24**, 183–196.

Kandler K (2004). Activity-dependent organization of inhibitory circuits: lessons from the auditory system. *Curr Opin Neurobiol* **14**, 96–104.

Kapfer C, Seidl AH, Schweizer H & Grothe B (2002). Experience-dependent refinement of inhibitory inputs to auditory coincidence-detector neurons. *Nat Neurosci* **5**, 247–253.

Karmarkar UR & Dan Y (2006). Experience-dependent plasticity in adult visual cortex. *Neuron* **52**, 577–585.

Katz LC & Shatz CJ (1996). Synaptic activity and the construction of cortical circuits. *Science* **274**, 1133–1138.

Keine C & Rübsamen R (2015). Inhibition shapes acoustic responsiveness in spherical bushy cells. *J Neurosci* **35**, 8579–8592.

Kim G & Kandler K (2003). Elimination and strengthening of glycinergic/GABAergic connections during tonotopic map formation. *Nat Neurosci* **6**, 282–290.

Kirkby LA, Sack GS, Firl A & Feller MB (2013). A role for correlated spontaneous activity in the assembly of neural circuits. *Neuron* **80**, 1129–1144.

Knudsen EI (2002). Instructed learning in the auditory localization pathway of the barn owl. *Nature* **417**, 322–328.

Kotak VC & Sanes DH (2000). Long-lasting inhibitory synaptic depression is age- and calcium-dependent. *J Neurosci* **20**, 5820–5826.

Kreinest M, Muller B, Winkelhoff J, Friauf E & Lohrke S (2009). Miniature EPSCs in the lateral superior olive before hearing onset. regional and cell-type-specific differences and heterogeneous neuromodulatory effects of ATP. *Brain Res* **1295**, 21–36.

Kros CJ, Ruppersberg JP & Rüsch A (1998). Expression of a potassium current in inner hair cells during development of hearing in mice. *Nature* **394**, 281–284.

Leake PA, Hradek GT, Chair L & Snyder RL (2006). Neonatal deafness results in degraded topographic specificity of auditory nerve projections to the cochlear nucleus in cats. *J Comp Neurol* **497**, 13–31.

Leao RN, Berntson A, Forsythe ID & Walmsley B (2004). Reduced low-voltage activated K^+ conductances and enhanced central excitability in a congenitally deaf (dn/dn) mouse. *J Physiol* **559**, 25–33.

Leao RN, Svahn K, Berntson A & Walmsley B (2005). Hyperpolarization-activated (I) currents in auditory brainstem neurons of normal and congenitally deaf mice. *Eur J Neurosci* **22**, 147–157.

Lewis C, Neidhart S, Holy C, North RA, Buell G & Surprenant A (1995). Coexpression of P2X2 and P2X3 receptor subunits can account for ATP-gated currents in sensory neurons. *Nature* **377**, 432–435.

Li M, Silberberg SD & Swartz KJ (2013). Subtype-specific control of P2X receptor channel signaling by ATP and Mg^{2+}. *PNAS* **110**, E3455–3463.

Lippe WR (1994). Rhythmic spontaneous activity in the developing avian auditory system. *J Neurosci* **14**, 1486–1495.

Lu T & Trussell LO (2007). Development and elimination of endbulb synapses in the chick cochlear nucleus. *J Neurosci* **27**, 808–817.

Malenka RC (1991). The role of postsynaptic calcium in the induction of long-term potentiation. *Mol Neurobiol* **5**, 289–295.

Manis PB & Marx SO (1991). Outward currents in isolated ventral cochlear nucleus neurons. *J Neurosci* **11**, 2865–2880.

Mann ZF & Kelley MW (2011). Development of tonotopy in the auditory periphery. *Hear Res* **276**, 2–15.

Markram H, Lübke J, Frotscher M & Sakmann B (1997). Regulation of synaptic efficacy by coincidence of postsynaptic APs and EPSPs. *Science* **275**, 213–215.

McCobb DP & Beam KG (1991). Action potential waveform voltage-clamp commands reveal striking differences in calcium entry via low and high voltage-activated calcium channels. *Neuron* **7**, 119–127.

McGinley MJ & Oertel D (2006). Rate thresholds determine the precision of temporal integration in principal cells of the ventral cochlear nucleus. *Hear Res* **216–217**, 52–63.

McKay SM & Oleskevich S (2007). The role of spontaneous activity in development of the endbulb of Held synapse. *Hear Res* **230**, 53–63.

Milenkovic I, Rinke I, Witte M, Dietz B & Rubsamen R (2009). P2 receptor-mediated signaling in spherical bushy cells of the mammalian cochlear nucleus. *J Neurophysiol* **102**, 1821–1833.

Milenkovic I, Witte M, Turecek R, Heinrich M, Reinert T & Rubsamen R (2007). Development of chloride-mediated inhibition in neurons of the anteroventral cochlear nucleus of gerbil (*Meriones unguiculatus*). *J Neurophysiol* **98**, 1634–1644.

Morest DK, Hutson KA & Kwok S (1990). Cytoarchitectonic atlas of the cochlear nucleus of the chinchilla, *Chinchilla laniger*. *J Comp Neurol* **300**, 230–248.

Muller M (1996). The cochlear place-frequency map of the adult and developing Mongolian gerbil. *Hear Res* **94**, 148–156.

Neher E (1992). Correction of liquid junction potentials in patch clamp experiments. *Methods Enzymol* **207**, 123–131.

North RA (2002). Molecular physiology of P2X receptors. *Physiol Rev* **82**, 1013–1067.

North RA & Surprenant A (2000). Pharmacology of cloned P2X receptors. *Annu Rev Pharmacol Toxicol* **40**, 563–580.

O'Leary DDM & McLaughlin T (2005). Mechanisms of retinotopic map development: ephs, ephrins, and spontaneous correlated retinal activity. *Prog Brain Res* **147**, 43–65.

Ostapoff EM, Feng JJ & Morest DK (1994). A physiological and structural study of neuron types in the cochlear nucleus. II. Neuron types and their structural correlation with response properties. *J Comp Neurol* **346**, 19–42.

Pankratov Y, Lalo U, Krishtal OA & Verkhratsky A (2009). P2X receptors and synaptic plasticity. *Neuroscience* **158**, 137–148.

Pankratov YV, Lalo UV & Krishtal OA (2002). Role for P2X receptors in long-term potentiation. *J Neurosci* **22**, 8363–8369.

Pfeiffer RR (1966). Classification of response patterns of spike discharges for units in the cochlear nucleus: tone-burst stimulation. *Exp Brain Res* **1**, 220–235.

Price GD & Trussell LO (2006). Estimate of the chloride concentration in a central glutamatergic terminal: a gramicidin perforated-patch study on the calyx of Held. *J Neurosci* **26**, 11432–11436.

Programs for Digital Signal Processing, Eds. Digital Signal Processing Committee of the IEEE Acoustics, Speech, and Signal Processing Society, New York: IEEE Press, 1979, chap. 8.

Rhode WS & Smith PH (1986). Encoding timing and intensity in the ventral cochlear nucleus of the cat. *J Neurophysiol* **56**, 261–286.

Rosenberg SS & Spitzer NC (2011). Calcium signaling in neuronal development. *Cold Spring HarbPerspect Biol* **3**, a004259.

Rouiller EM & Ryugo DK (1984). Intracellular marking of physiologically characterized cells in the ventral cochlear nucleus of the cat. *J Comp Neurol* **225**, 167–186.

Rubel EW & Fritzsch B (2002). Auditory system development. primary auditory neurons and their targets. *Annu Rev Neurosci* **25**, 51–101.

Rubio ME & Soto F (2001). Distinct localization of P2X receptors at excitatory postsynaptic specializations. *J Neurosci* **21**, 641–653.

Rubsamen R & Schafer M (1990). Ontogenesis of auditory fovea representation in the inferior colliculus of the Sri Lankan rufous horseshoe bat, Rhinolophus rouxi. *J Comp Physiol [A]* **167**, 757–769.

Rübsamen R (1992). Postnatal development of central auditory frequency maps. *J Comp Physiol [A]* **170**, 129–143.

Ryugo DK & Sento S (1991). Synaptic connections of the auditory nerve in cats: relationship between endbulbs of held and spherical bushy cells. *J Comp Neurol* **305**, 35–48.

Sanes DH & Bao S (2009). Tuning up the developing auditory CNS. *Curr Opin Neurobiol* **19**, 188–199.

Sanes DH & Constantine-Paton M (1983). Altered activity patterns during development reduce neural tuning. *Science* **221**, 1183–1185.

Sanes DH & Constantine-Paton M (1985). The sharpening of frequency tuning curves requires patterned activity during development in the mouse, *Mus musculus*. *J Neurosci* **5**, 1152–1166.

Sanes DH & Siverls V (1991). Development and specificity of inhibitory terminal arborizations in the central nervous system. *J Neurobiol* **22**, 837–854.

Sanes DH & Takacs C (1993). Activity-dependent refinement of inhibitory connections. *Eur J Neurosci* **5**, 570–574.

Seidl AH & Grothe B (2005). Development of sound localization mechanisms in the mongolian gerbil is shaped by early acoustic experience. *J Neurophysiol* **94**, 1028–1036.

Shah RD & Crair MC (2008). Mechanisms of response homeostasis during retinocollicular map formation. *J Physiol* **586**, 4363–4369.
Song S, Miller KD & Abbott LF (2000). Competitive Hebbian learning through spike-timing-dependent synaptic plasticity. *Nat Neurosci* **3**, 919–926.
Sonntag M, Englitz B, Kopp-Scheinpflug C & Rubsamen R (2009). Early postnatal development of spontaneous and acoustically evoked discharge activity of principal cells of the medial nucleus of the trapezoid body: an in vivo study in mice. *J Neurosci* **29**, 9510–9520.
Taschenberger H & Gersdorff Hvon (2000). Fine-tuning an auditory synapse for speed and fidelity: developmental changes in presynaptic waveform, EPSC kinetics, and synaptic plasticity. *J Neurosci* **20**, 9162–9173.
Tritsch NX & Bergles DE (2010). Developmental regulation of spontaneous activity in the mammalian cochlea. *J Neurosci* **30**, 1539–1550.
Tritsch NX, Rodriguez-Contreras A, Crins TT, Wang HC, Borst JG & Bergles DE (2010). Calcium action potentials in hair cells pattern auditory neuron activity before hearing onset. *Nat Neurosci* **13**, 1050–1052.
Tritsch NX, Yi E, Gale JE, Glowatzki E & Bergles DE (2007). The origin of spontaneous activity in the developing auditory system. *Nature* **450**, 50–55.
Typlt M, Englitz B, Sonntag M, Dehmel S, Kopp-Scheinpflug C & Ruebsamen R (2012). Multidimensional characterization and differentiation of neurons in the anteroventral cochlear nucleus. *PloS ONE* **7**, e29965.
Typlt M, Haustein MD, Dietz B, Steinert JR, Witte M, Englitz B, Milenkovic I, Kopp-Scheinpflug C, Forsythe ID & Rubsamen R (2010). Presynaptic and postsynaptic origin of multicomponent extracellular waveforms at the endbulb of Held-spherical bushy cell synapse. *Eur J Neurosci* **31**, 1574–1581.
Virginio C, North RA & Surprenant A (1998). Calcium permeability and block at homomeric and heteromeric P2X2 and P2X3 receptors, and P2X receptors in rat nodose neurones. *J Physiol* **510**, 27–35.
Volonte C, Amadio S, D'Ambrosi N, Colpi M & Burnstock G (2006). P2 receptor web: complexity and fine-tuning. *Pharmacol Ther* **112**, 264–280.
Walmsley B, Berntson A, Leao RN & Fyffe RE (2006). Activity-dependent regulation of synaptic strength and neuronal excitability in central auditory pathways. *J Physiol* **572**, 313–321.
Watano T, Calvert JA, Vial C, Forsythe ID & Evans RJ (2004). P2X receptor subtype-specific modulation of excitatory and inhibitory synaptic inputs in the rat brainstem. *J Physiol* **558**, 745–757.
Werthat F, Alexandrova O, Grothe B & Koch U (2008). Experience-dependent refinement of the inhibitory axons projecting to the medial superior olive. *Dev Neurobiol* **68**, 1454–1462.
White LE & Fitzpatrick D (2007). Vision and cortical map development. *Neuron* **56**, 327–338.
Woolf NK & Ryan AF (1984). The development of auditory function in the cochlea of the mongolian gerbil. *Hear Res* **13**, 277–283.
Wright S, Hwang Y & Oertel D (2014). Synaptic transmission between end bulbs of Held and bushy cells in the cochlear nucleus of mice with a mutation in Otoferlin. *J Neurophysiol* **112**, 3173–3188.
Young ED, Robert JM & Shofner WP (1988). Regularity and latency of units in ventral cochlear nucleus: implications for unit classification and generation of response properties. *J Neurophysiol* **60**, 1–29.
Zhang W & Linden DJ (2003). The other side of the engram: experience-driven changes in neuronal intrinsic excitability. *Nat Rev Neurosci* **4**, 885–900.
Zucker RS (1999). Calcium- and activity-dependent synaptic plasticity. *Curr Opin Neurobiol* **9**, 305–313.

Additional information

Competing interests

The authors declare that they have no competing interests.

Author contributions

SSS, RR and IM provided funding, conceived the experiments and wrote the manuscript. SJ, TR, CC, BD and JN acquired and analysed the data and revised the manuscript critically for important intellectual content. All authors approved the final version of the manuscript, and agree to be accountable for all aspects of the work in ensuring that questions related to the accuracy or integrity of any part of the work are appropriately investigated and resolved. All persons designated as authors qualify for authorship, and all those who qualify for authorship are listed.

Funding

This work was supported by the DFG grants MI 954/3-1, MI 954/2-1 (IM), RU 390/19-1 (RR and JN), GRK 1097 (BD), the Intramural Research Program of the National Institute of Child Health and Human Development (CC and SSS) and a DAAD scholarship to SJ.

Acknowledgements

We thank Christian Keine for valuable help regarding analyses.